Heliyon 9 (2023) e20032

Contents lists available at ScienceDirect

Heliyon

journal homepage: www.cell.com/heliyon

Facies analysis, biostratigraphy, and provenance of the late Neogene Seulimeum Formation, Northwest Aceh basin, Sumatra (Indonesia)

Gartika Setiya Nugraha [a,b,*], Edy Sunardi [b], Iyan Haryanto [b], Billy Gumelar Adhiperdana [b], Rakhmat Fakhruddin [c], Ria Fitriany [b], Dina Gunarsih [a]

[a] Geological Engineering, Faculty of Engineering, Universitas Syiah Kuala, Banda Aceh, 23111, Indonesia
[b] Faculty of Geology Engineering, Universitas Padjadjaran, Jln. Raya Bandung Sumedang Km 21, Jatinangor, 45363, Indonesia
[c] Research Center for Geological Resources, National Research and Innovation Agency, Jln. Cisitu, Sangkuriang Bandung, Jawa Barat, 40135, Indonesia

ARTICLE INFO

Keywords:
Seulimeum formation
Late neogene
Northwest Aceh Basin
Great Sumatran Fault
Barisan mountains range
Sumatra

ABSTRACT

A sedimentological, biostratigraphic, and petrographical investigation was conducted on exposed sedimentary rocks in the Seulimeum Formation in the Northwest Aceh Basin, Sumatra. Sedimentary facies analysis suggests a deep-marine depositional environment consists of an inner fan, middle fan, and outer fan to basin plain deposits. New foraminiferal data designated a late Miocene to early Pleistocene age for the studied rock unit, equivalent to N17 to N21 zone, with paleobathymetry in the bathyal environment. Petrographically, the sandstone of the Seulimeum Formation is included as subarkose, sublithic arenite, and lithic arenite, or classified as litho-quartzose, feldspatho-litho-quartzose, and litho-feldspatho-quartzose. Provenance analysis suggests that the origin of the sandstones is from the arc orogen sources. Furthermore, it is concluded that the development of the GSF zone in the late Neogene controls the formation of the deep-marine depositional setting. The west-south-west part of the fault is the footwall part (the Barisan Mountains), as the main high area of sedimentary source material consisting dominantly of the Woyla Group, with some contributions from Bentaro volcanic and Paleogene to early Neogene sediments. Our findings also suggest that the beginning of the Great Sumatran Fault, which corresponds with the uplift of the Barisan Mountains in the northern part of Sumatra, took place in the late Miocene, between 8.6 and 5.9 Ma.

1. Introductions

The research area is situated on the northern tip of Sumatra Island, known as Northwest Aceh Basin (Fig. 1). Recent work by Ghosal et al. [1] named the area as Breueh Basin, elongated NW-SE from the offshore Andaman Sea to the onshore south of Banda Aceh. The Breueh Basin is bounded by two main faults, the Aceh and the Seulimeum Fault, with a sediment thickness of more than 2 km [1]. These two faults are considered part of the Great Sumatran Fault (GSF) in their most northern domain [1,2]. In the Sumatra subduction system, the GSF and their Barisan Mountains range form an outstanding feature extending for 1700 km along the island's length from

* Corresponding author. Geological Engineering, Faculty of Engineering, Universitas Syiah Kuala, Banda Aceh, 23111, Indonesia.
E-mail address: setiya@usk.ac.id (G.S. Nugraha).

https://doi.org/10.1016/j.heliyon.2023.e20032
Received 13 June 2023; Received in revised form 7 September 2023; Accepted 8 September 2023
Available online 14 September 2023

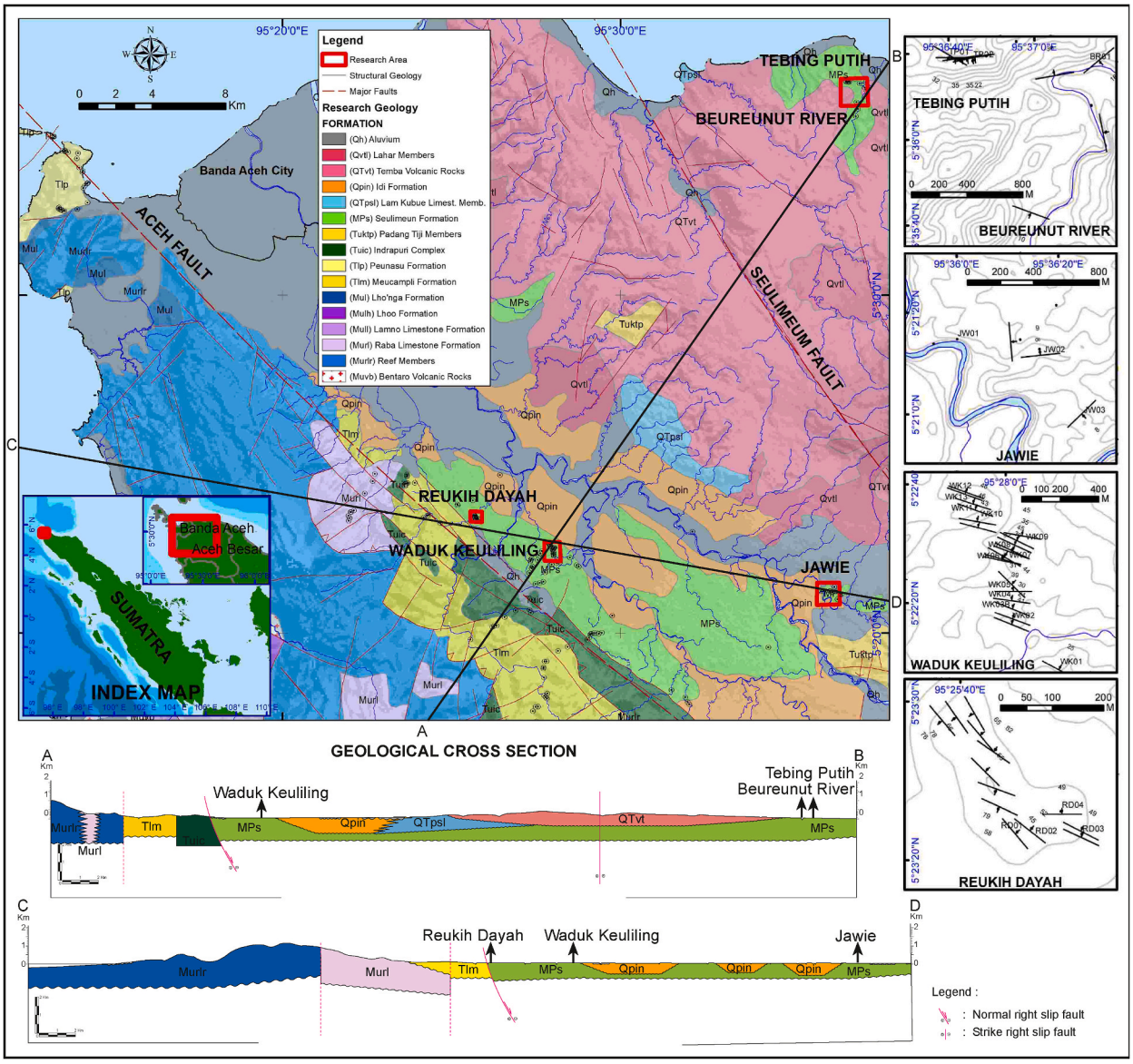

Fig. 1. The geological map of the Banda Aceh, Sumatra, shows the position of the outcrop measured sections: Tebing Putih, Beureunut River, Jawie, Waduk Keuliling, and Reukih Dayah (modified from Bennett et al. [6]).

the Andaman Sea to Sunda Strait [3,4]. The GSF is a major dextral transcurrent fault zone formed due to the oblique convergence between the Indian and Eurasian with Australian plates [2,5]. The initiation of the GSF as a transform fault is taught to be related to the opening of the Andaman Sea spreading system [3,5].

However, the time of the initiation of this fault zone is still a matter of continual speculation. Barber & Crow [3] and Ghosal et al. [1] suggest that it was initiated in the Middle Miocene (about 15–13 Ma), while Sieh and Natawidjaja [2] and Curray [5] supposed that the fault system may not be older than four ma (Pliocene). We hypothesized that one method to determine the age of the initiation of the GSF is by dating the age of sediment in the onshore part of the Breueh Basin, which is thought of as formed due to the initiation of the GSF.

One of the sand-prone rock formations in the study area that attracts our attention is the Seulimeum Formation. This unit is widespread in the study area, from the Reukih Dayah in the west to the Tebing Putih area in the east. In the regional geological map of the Banda Aceh area by Bennett et al. [6], the Seulimeum Formation was mapped as Quaternary in age and reported to have a thickness of around 500 m. Furthermore, in the study area, several of the exposed Tertiary rocks are the equivalents of the rock unit that include an important petroleum system from the adjacent producing basin, the onshore North Sumatra Basin in the southeast, and the offshore Mergui Basin in the northeast [7–11]. Both hydrocarbon-producing basins have the Neogene clastic sediment as one of their main reservoirs [7,8]. However, to the best of our knowledge, there is only limited published work about the Neogene clastic sediments from

the Northwest Aceh/Breueh Basin. Therefore, we planned fieldwork to re-mapped and re-dating this representative sandstone rock unit (the Seulimeum Formation).

This paper reports the result of the recent fieldwork mapping, including the lithofacies, biostratigraphy, and petrography analysis of the Seulimeum Formation in the Breueh Basin. The aims of this paper are (1) to describe the lithofacies characteristics and their depositional environment interpretation, (2) to establish a new biostratigraphic dating and paleo bathymetry information based on the recovered foraminifera, (3) to document the petrographic texture and composition of the sandstone as well as their provenance and tectonic setting interpretation, (4) to integrate and discuss all the findings into the history of the late Neogene basin forming and basin filling interpretations.

2. Geological setting

The regional geological information of the study area and surrounding area is provided mainly by Bennett et al. [6], with recent Tertiary volcanic rocks dating by Lai et al. [12] (Fig. 2). Late Jurassic to early Cretaceous Woyla Group act as the basement for the Tertiary succession above them. It is divided into two successions of a rather different lithology and structural complexity named the western and eastern Woyla Group. The westerly part consists of low-grade metavolcanic, volcanogenic sediments and recrystallized limestones. The more easterly succession is more complex and frequently severely tectonised, which comprises metabasalts, red radiolarian cherts, meta-limestones, and metarudites is overlain by slates, metavolcanic and volcanogenic sediments in places spatially associated with serpentinites.

The Tertiary succession is started by the Eocene to early Oligocene Meucampli Formation and consists of sandstones and conglomerates with sub-ordinate siltstones, mudstones, and minor limestones. Locally intermediate to mafic volcanic is also present. This sediment depositional environment was considered paralic to fluvial and partly deltaic sediment. Above them was the late Oligocene to early Miocene Peunasu Formation, which consisted of reef limestone overlying micaceous sandstones and laminated siltstones and mudstones. Their environment of deposition is from an open marine setting to a paralic-fluvial part.

The next in the succession is the early to middle Miocene Baro Formation. It comprises calcareous siltstone and mudstone with minor sandstone and limestone deposited in an open marine setting. The Pliocene Padang Tiji Member is overlying the Baro Formation. It

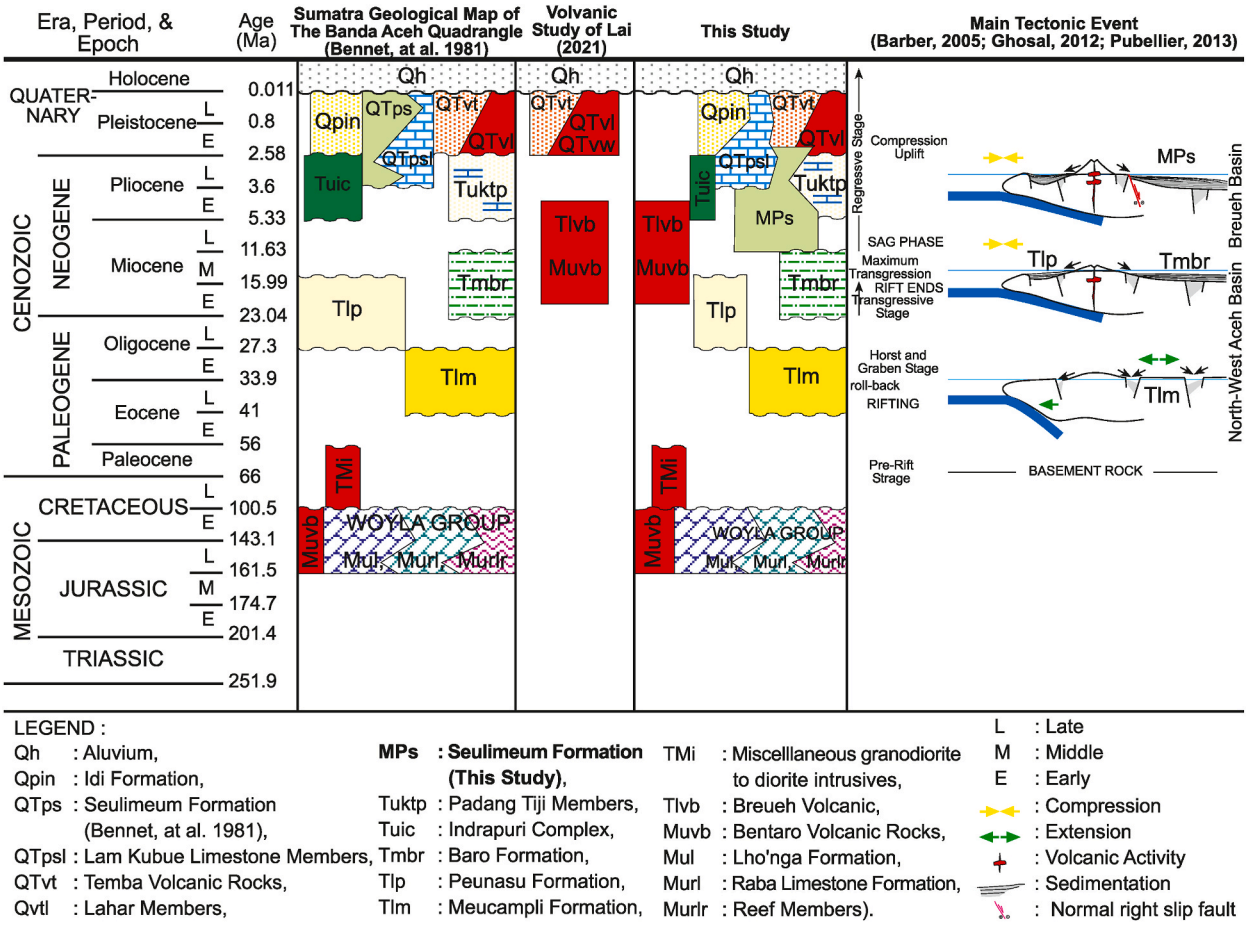

Fig. 2. Generalized stratigraphic column of the Banda Aceh area and surrounding [1,6,12,13,14].

consists of calcareous sandstones and conglomerates with minor mudstones and limestones deposited in the open marine environment. The last sedimentary succession in the study area is the Quaternary deposit consisting of various clastic sediment and limestone types.

3. Materials and methods

This study is based on the exposed rock unit along the river, cliff, and roadside from five locations (Reukih Dayah, Waduk Keuliling, Jawie, Beureunut River, dan Tebing Putih) of the Northwest Aceh/Breueh Basin, Aceh, Indonesia (Fig. 1), namely the Seulimeum Formation. Three methods were used that is lithofacies, biostratigraphy, and petrography analysis. The lithofacies analysis performed in this study consists of describing the sedimentary rocks in the field and their classification and interpretation into facies and facies association based on Anderton [15] and Dalrymple [16]. The sedimentary rock unit's description included lithology, grain size, sedimentary structures, texture, and bed contact. It was then recorded into composite stratigraphic logs for each observation location, totaling 385 m succession. The classification was based on the sedimentary features that were thought to have genetic significance, which in this study was defined mainly based on grain size, sedimentary structures, and texture. The closely related lithofacies are then grouped into facies associations which are considered to represent a distinctive sub-environment. The interpretations of facies associations were mainly based on Nichols [17], Posamentier and Walker [18], Shanmugam [19], Talling et al. [20,21], Kane et al. [22], and Botziolis et al. [23].

Biostratigraphic (foraminifera) analysis was performed on 18 representative fine-grained samples from five studied sections. One hundred grams per sample was crushed and then soaked in 10% hydrogen peroxide (H_2O_2) solution added, which was added with 1.5 g NaOH to accelerate the reaction (e.g., Ref. [24]). The samples were soaked until they did not react for approximately 8–12 h. After that, the samples were washed with running water and filtered with a mesh size of 120. After being filtered, the samples were dried in an oven for about 4–8 h until completely dry. After drying, samples were taken weighing 1 g to separate the sediment and the fossils. Separation of fossils and sediments using a binocular microscope with a magnification of 40×. After being separated, the foraminifera fossils were determined and attached to the microfossil preparations while counting the number of each individual of each species. After that, representative fossil for each species was photographed using the microscope and the Zen 2.0 photo application. Local biozonation is established based on first appearance datum (FAD) and last appearance datum (LAD) of foraminifera index species (e.g., Ref. [25]). The schemes of Blow [26] and Wade et al. [27] were adopted for age determination. Paleobathymetry interpretation using benthic foraminifera was based on Berggren [28], Hedgpeth [29], Ingle [30], and Murray [31].

A total of 14 medium to coarse-sized sandstone samples were collected for petrographic analysis. The samples were prepared as thin sections (2.5 × 4 cm) and studied using an optical microscope at Universitas Padjadjaran, Bandung, and Universitas Syiah Kuala, Aceh. The petrographic analysis comprised identifying the compositional of the clasts, characterization of the sandstone, their textural, and the modal data analysis (e.g., Refs. [32,33]). Observation of the sandstone texture consists of measurements of grain size, grain contact, roundness, sorting, as well as internal and fabric arrangement. The grain-size scale was used of Wentworth [34] and Blair and McPherson [35], while sorting and roundness used visual comparison charts of Compton [36] and Powers [37]. The modal analysis was utilized by the hybrid-point counting method, which combines the criteria and petrographic categories of the classic method (QFR) and the Gazzi-Dickinson method (QFL) (e.g., Ref. [38]). A total of 1000 points per thin section were counted with the counting grid settled with a 2 mm vertical and 1/3 mm horizontal separation. The sandstones classification was using the Q-F-R diagram of Pettijohn [39] and the Q-F-L diagram of Garzanti [40] (e.g. Ref. [41], Qt-F-L and Qm-F-Lt triangular diagrams of Dickinson [42] and Dickinson et al. [43] were used to establish the provenance.

4. Results and discussions

4.1. Lithofacies

All the studied rock units are included in the Seulimeum Formation. Based on lithology, sedimentary features, and bedding characteristics, the Seulimeum Formation could be classified into eight different lithofacies (Table 1; Figs. 3–5). Their lithological characteristic is described as follow.

4.1.1. Conglomerate (F1)

Facies F1 comprises disorganized or structureless matrix-supported conglomerates with various clasts of igneous and metamorphic rocks, quartz, and sandstone (Fig. 6A–D). The clasts are subangular to angular with a size of 5 mm to 25 cm, and they are scattered randomly with rare imbrication. Their matrix is mainly medium-to coarse-grained sand. The basal contacts of these facies are sharp to erosional with irregular upper contact. The conglomerate facies thickness varies from 25 cm to 5 m. These facies are present in the Waduk Keuliling location.

4.1.2. Conglomeratic sandstone (F2)

These facies consist of medium-to coarse-grained sand with subangular to angular granule-to-pebble clasts (Fig. 6E–G). They commonly show normal grading and massive bedding. Inverse to normally graded, crude horizontal stratification and imbrication of clasts are observed locally. The clasts are also composed of igneous and metamorphic rock, sandstone, and quartz and are dominantly in random fabric. These facies shows gradational upper contact with sharp basal contact. This individual facies bed varies in thickness from 10 cm to 1 m. They can be observed in Reukih Dayah and Waduk Keuliling locations.

Table 1
Lithofacies classification.

	Facies	Textures	Structures
F1	Conglomerate	Clasts comprised of igneous and metamorphic rocks, quartz, and sandstone. They are subangular to angular with a size of 5 mm to 25 cm. Matrix is mainly represented by medium- to coarse-grained sandstone	Disorganized or structureless
F2	Conglomeratic sandstone	Medium- to coarse-grained sandstone with subangular to angular granule-to-pebble clasts. Clasts consist of igneous rock, metamorphic rock, sandstone, and quartz	Commonly normal grading and massive bedding. Inverse to normally graded, crude horizontal stratification and imbrication of clasts are observed locally
F3	Thick-bedded sandstone	Medium- to coarse-grained sandstone with moderate to poorly sorting. Amalgamated beds up to 5 m thick, with rare thin mudstone partings between beds	Mostly massive, with parallel and cross-lamination found locally. Uncommon graded bedding and dish structures are observed in places
F4	Sandstone to mudstone heterolithics	Centimeter to decimeters alternating bed of sandstone, siltstone, and mudstone. The sandstones are very fine- to fine-grained	Overall normal grading form from the sandstone to siltstone and mudstone. The sandstone show structureless, parallel lamination, ripple cross-lamination, and normal grading structures
F5	Slumped sandstone	Fine- to coarse-grained sandstone with moderate to poorly sorting	Deformed bedding
F6	Siltstone	Sandy siltstone with intercalation of laminated to thinly bedded very fine-grained sandstone	Massive to faintly laminated, thickly bedded
F7	Claystone	Claystone with intercalation of laminated to centimeters bedded of very fine-grained sandstone	Massive, thickly bedded
F8	Sandy tuff	Centimeter to decimeter bedded of sandy tuff	Parallel bedding

4.1.3. Thick-bedded sandstone (F3)

The F3 facies is composed of moderate to poorly sorted medium-to coarse-grained sandstone (Fig. 7A–D). These facies are primarily massive, with parallel and cross-lamination found in places. The sandstone is commonly stacks of amalgamated beds up to 5 m thick, with rare thin mudstone partings between beds. Individual bed thickness range from 30 cm to 1 m. Uncommon graded bedding and dish structures are found locally. The facies display sharp basal and upper contacts. These facies are present in all studied sections but most commonly occur in Waduk Keuliling. Some sandstone layers have tuffaceous nature, which is generally found at the Tebing Putih and Beureunut River locations.

4.1.4. Sandstone to mudstone heterolithics (F4)

These facies include monotonous successions of a centimeter to decimeters alternating sandstone, siltstone, and mudstone bedded (Fig. 8A–D). The sandstones are very fine-to fine-grained, sharp to erosional centimeter scale bases that include scour and tool marks. They are in the form of structureless, parallel, or ripple cross-lamination. Some sandstone beds are also tuffaceous. The interbedded siltstone and mudstone are commonly dark grey and have massive to faint lamination. Overall this facies shows a normal grading form from the sandstone above to the siltstone and mudstone layer at the top. The facies are up to 7 m in thickness. They are found in all four locations but are most common at Tebing Putih and Beureunut River.

4.1.5. Slumped sandstone (F5)

The slumped sandstone facies consist of deformed beds of fine-to coarse-grained sandstone, moderate to poorly sorted (Fig. 8E–H). Some sandstone beds are tuffaceous. These facies are characterized by the slumped horizon between normal undeformed bedding below and above it. The deformed beds are up to 10 m thick and are found in Reukih Dayah and Waduk Keuliling.

4.1.6. Siltstone (F6)

These facies are observed in Waduk Keuliling and Jawie locations. It is composed of sandy siltstone with intercalation of laminated to thinly bedded very fine-grained sandstone (Fig. 9A–D). The siltstone is massive to faintly laminated, thickly bedded, ranging from 50 cm to a total of 12 m thickness. It is primarily calcareous and sometimes contains plant, mollusks, and larger foraminifera debris. The sandstone as intercalation ranges from less than 1 cm to several centimeters and shows cross to parallel lamination structures.

4.1.7. Claystone (F7)

The claystone facies mainly consist of thickly bedded, massive, light to brownish-grey claystone (Fig. 9E–F). This facies thickness ranges from two to 8 m. Intercalation of laminated to centimeters bedded of very fine-grained sandstone is locally observed. The sandstone also shows cross-to-parallel lamination structures. The claystone facies is also found in Waduk Keuliling and Jawie location.

4.1.8. Sandy tuff (F8)

The sandy tuff facies consist of a centimeter to decimeter bedded of white to light brown sandy tuff (Fig. 8A and B). Some layers are calcareous. These facies are mostly found in the Tebing Putih and Beureunut River locations with a thickness of up to 3,5 m. In the Waduk Keuliling location, these facies are rarely found as intercalation between the thickly bedded sandstone up to 10 cm thick.

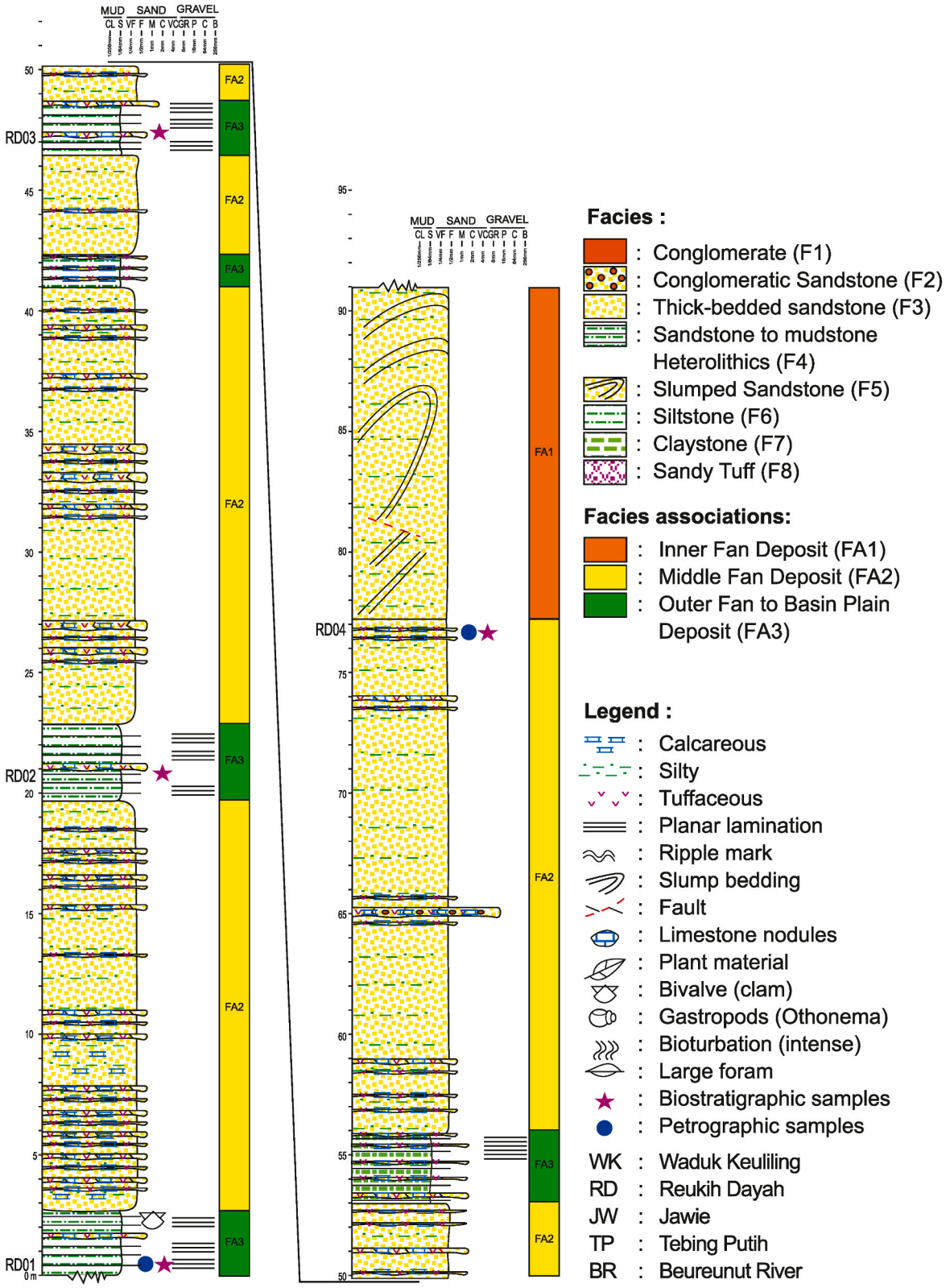

Fig. 3. Stratigraphic logs in the succession of Reukih Dayah location.

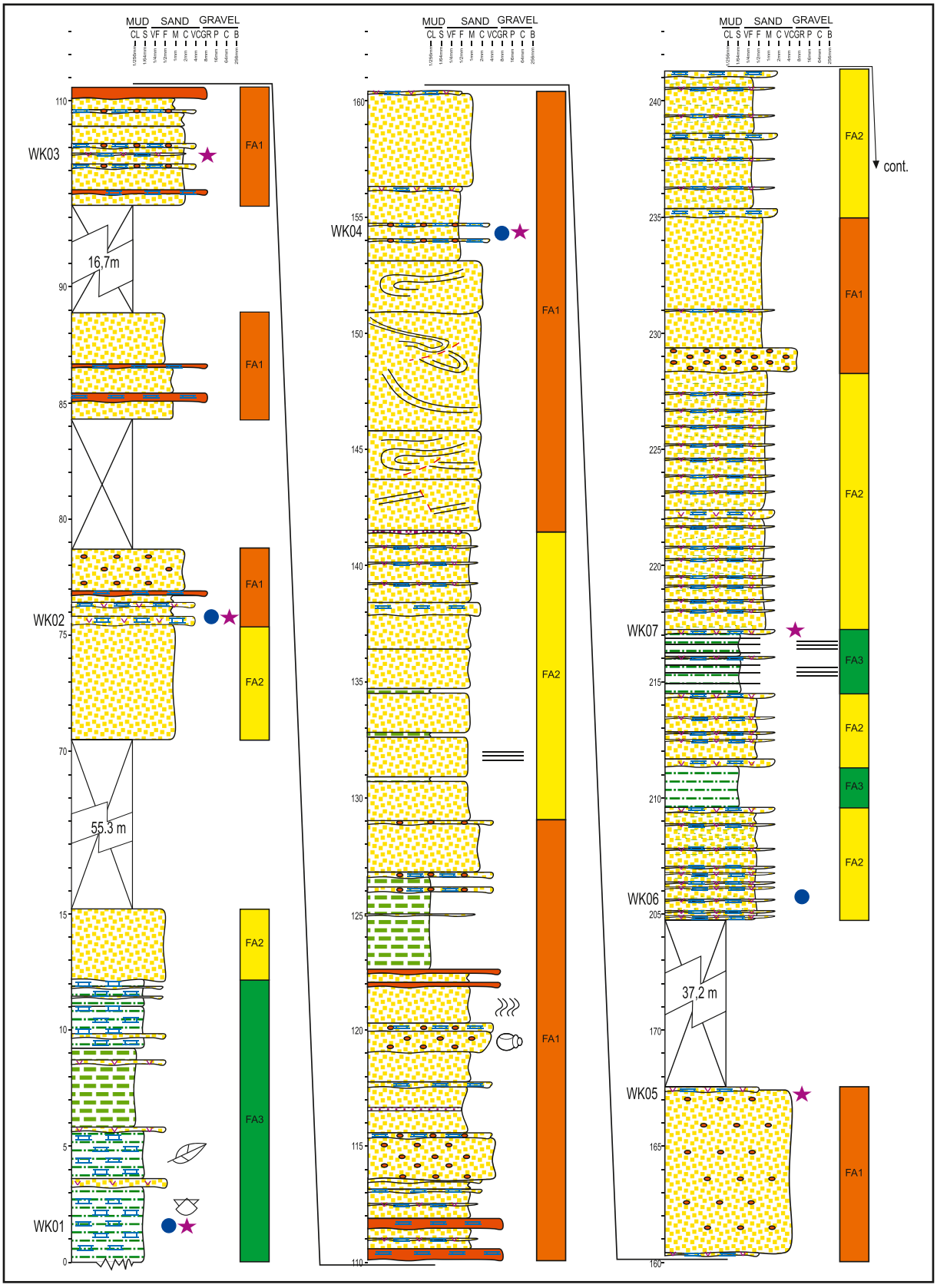

Fig. 4. Stratigraphic logs in the succession of Waduk Keuliling location.

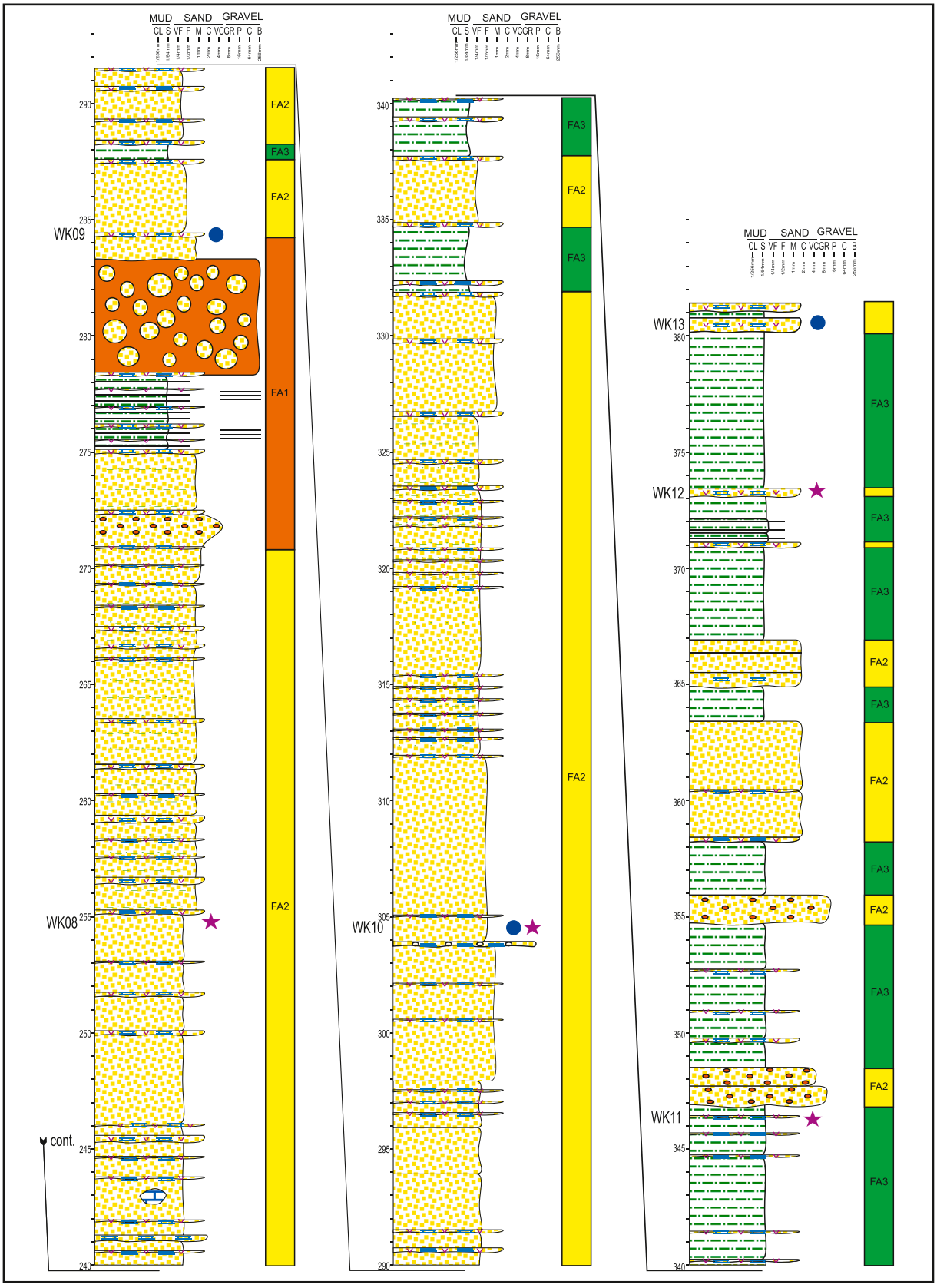

Fig. 4. (*continued*).

4.2. Facies association

The facies that are closely related and have intimate physical associations are combined into facies associations. From the eight recognized lithofacies, it could then be grouped into three facies associations (Figs. 3–5). Each of the FA is thought to correspond to a unique depositional environment. Overall, the studied rock section is interpreted to represent deep marine deposits accumulated in submarine fan systems [17,18,20–23,44,45]. Their description and interpretation is as follows.

4.2.1. Inner fan deposit (FA1)

4.2.1.1. Description. FA1 is consist of F1, F2, F3, F4, and F5. A fining-upward pattern of F1, F2 to F3 is commonly observed. These units are amalgamated together and develop several tens of meters thick of successions. In this FA, F4 and F5 occurred as a minor intercalation constituent between the thick conglomerate and sandstone successions (F1 – F3). The FA1 reaches a total of 14–25 m thick and is laterally discontinuous. This facies association is frequently found interbedded with FA2. FA1 is only observed in the Waduk Keuliling location.

4.2.1.2. Interpretation. FA1 can be divided into two subdeposits: the channel-fill and channel-levee deposits. The channel fill deposit is characterized by thick conglomerate and sandstone (F1 – F3), which commonly display a fining-upward pattern. The channel-levee deposit is represented by thin-bedded sandstone to mudstone (F4). The slumped facies (F5) suggest accumulation on an unstable sloping surface. Rapid deposition of sandstone with trapped pore water followed by failure of the sandstone beds along a weak layer with high pore pressure may result in the sediments' movement by a few meters. Consequently, the deposited unit would be identified as a slump [19]. The upper part of the submarine fan or along the base of the slope is the probable deposition area of these slumped sandstone facies [46,47]. Overall, FA1 is inferred as accumulated in the inner fan environment, where strong turbidity currents are confined to the channels. This inner fan sub-environment in the submarine fan systems is marked by the presence of the coarsest sediment in the system [48,49].

4.2.2. Middle fan deposit (FA2)

4.2.2.1. Description. FA2 is comprised chiefly of F3 with the additional constituent of F2 and F8. The stacked thick-bedded sandstone of F3 displays an overall coarsening- and thickening-upward succession. Between the stacked sandstone succession, the interbedded conglomeratic sandstone facies of F2 are commonly found, while the occurrence of sandy tuff (F8) is rarely observed. The amalgamation of this facies association may reach up to 45 m in thickness. Lateral continuity (10s of m) of this FA is locally observed. FA2 is interbedded with FA1 and FA3. This unit was studied at Reukih Dayah, Waduk Keuliling, Tebing Putih, and Beureunut River locations.

4.2.2.2. Interpretation. The thick-bedded sandy turbidites (F3), which show an overall coarsening-up and thickening-up succession, typify the middle fan deposit [17,48,50]. This feature is thought as the result of depositional lobe progradation. The other deposit which occurs in this FA is the conglomeratic sandstone facies of F2, which are interpreted as channel deposits on the lobe of the middle fan area. F8 (sandy tuff) rarely occurred as intercalation between the thick sandstone interval, interpreted as representing a pyroclastic event during the deposition of the submarine fan system. In summary, FA2 is suggested as the middle fan deposits.

4.2.3. Outer fan to basin plain deposit (FA3)

4.2.3.1. Description. FA3 is characterized by the presence of fine-grained sediments of F4, F6, F7, and F8. The sandstone to mudstone heterolithics facies of F4 is commonly found interbedded with siltstone and claystone facies of F6 and F7. The sandy tuff facies of F8 are present as a rare intercalation. Tens of meters of lateral continuity of this FA are found in places. The thickness of this FA is up to 33 m. FA3 was found at Reukih Dayah, Waduk Keuliling, Tebing Putih, Beureunut River, and Jawie locations.

4.2.3.2. Interpretation. This FA is thought to represent the deposit of the distal parts of the submarine fan. The F4 (sandstone to mudstone heterolithics) is interpreted as turbidite sheets deposits, while the massive siltstone and mudstone (F6 and F7) are considered as the interbedded hemipelagic deposit [17,51]. The F8 (sandy tuff) is inferred as the deposit of pyroclastic events around the deposition site. FA3 is concluded as the outer fan to basin plain deposit in a submarine fan setting which is characterized by the occurrence of the finest sediment in the system [48,49].

4.3. Foraminifera analysis

From 18 analyzed samples, three are barren of foraminifera, while the other 15 samples yielded good preservation of planktonic and benthonic foraminifera. The fossils found in the 15 samples are abundant, above 100 specimens per sample. A total of 62 distinct foraminifera types were recorded from the studied samples, consisting of 23 planktonic types and 39 bentonic forms (Table 2).

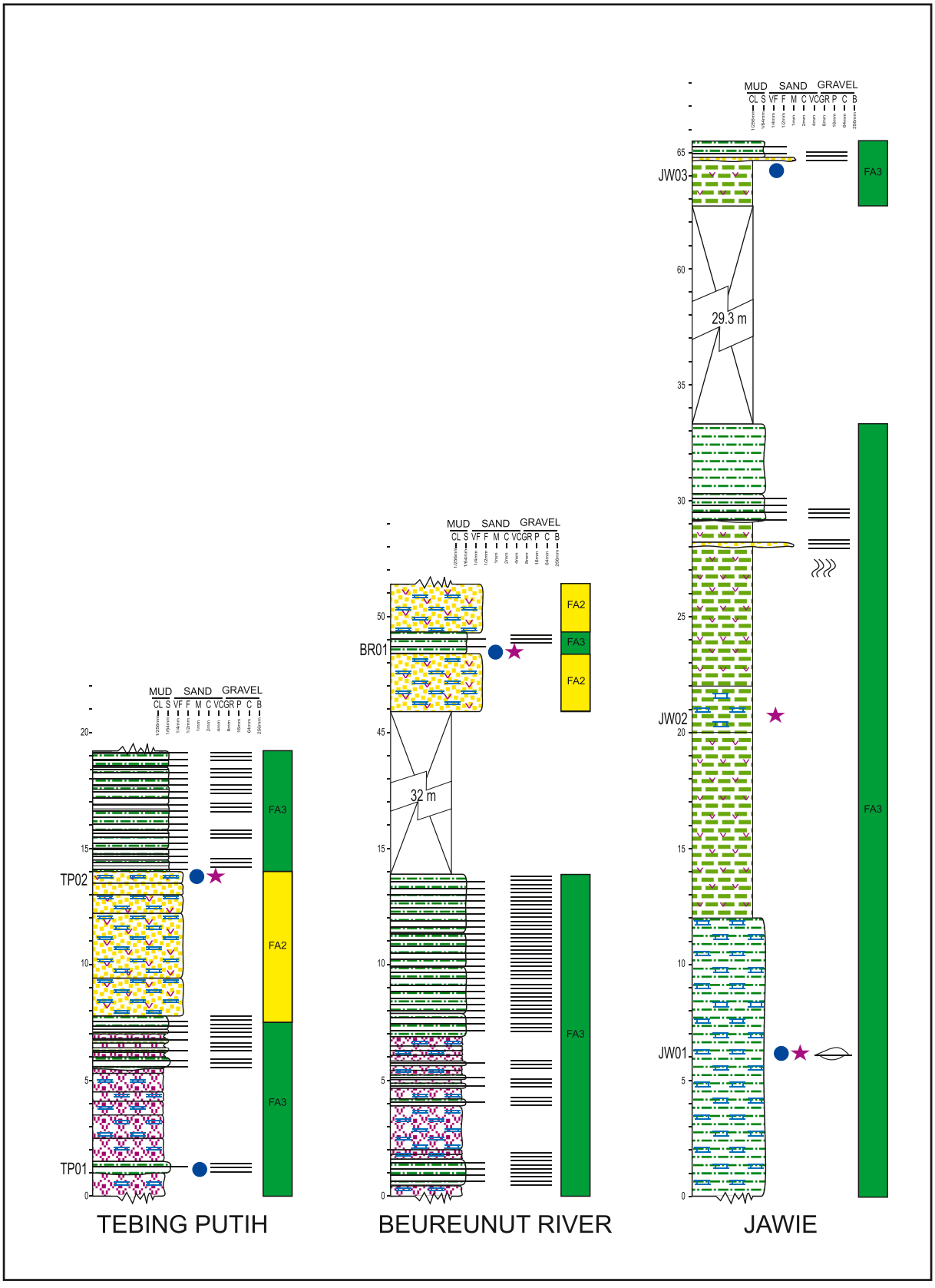

(caption on next page)

Fig. 5. Stratigraphic logs in the succession of Tebing Putih, Beureunut River, and Jawie locations.

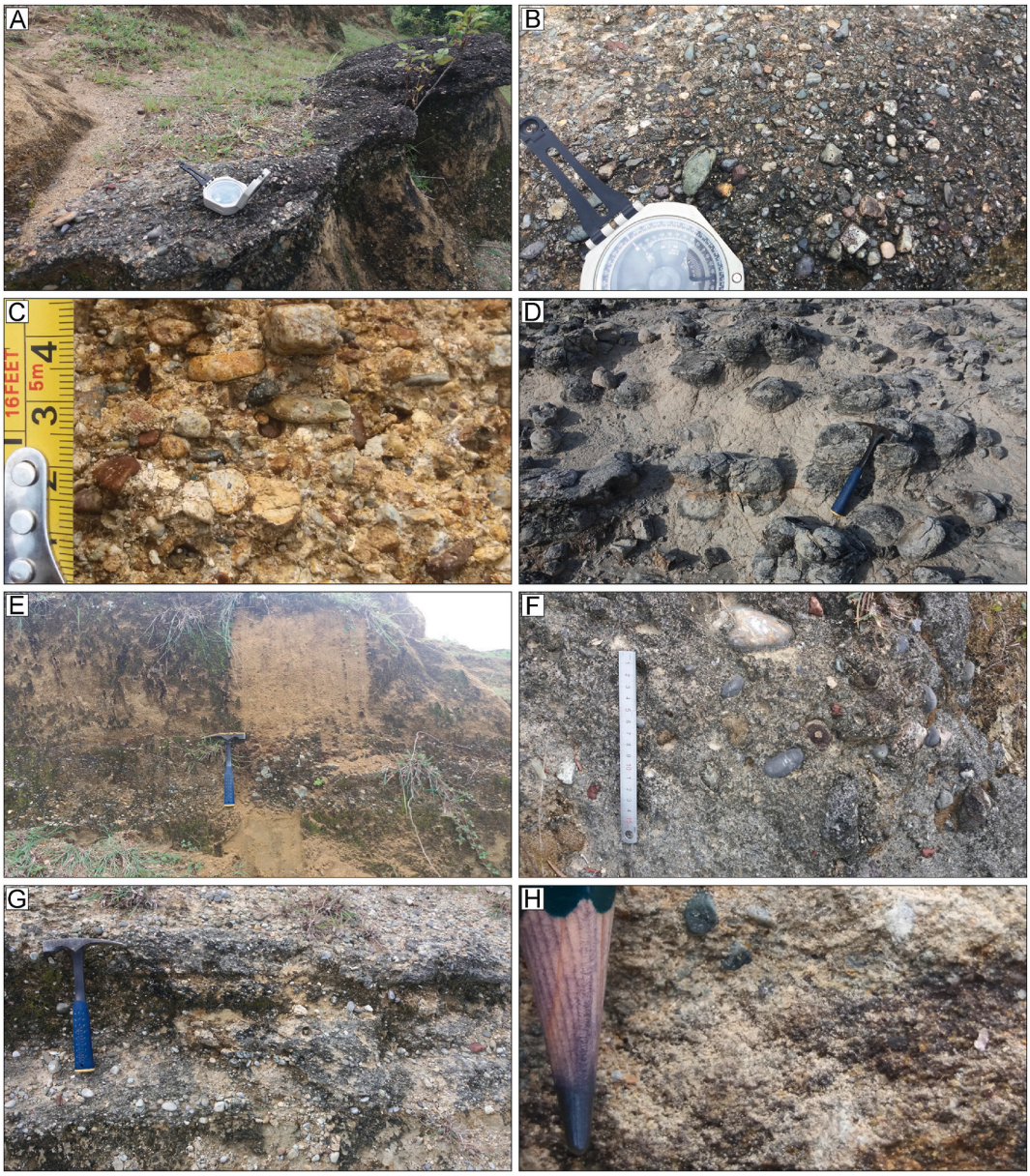

Fig. 6. Outcrop expression of facies F1 and F2 (hammer is ca. 25 cm long): A) Conglomerate layers erosional basal contacts; B, C) Conglomerate with igneous rock clasts and black minerals; D) Conglomerate with sandstone clasts; E) Conglomeratic sandstone with irregular upper contact underlying by sandstone layer; F) Conglomeratic sandstone with gravel to cobble-sized clasts, rounded to subangular shapes, including igneous rock fragments, quartz minerals, and black minerals; G) Conglomeratic sandstone with pebble-sized clasts; H) Conglomeratic sandstone poorly sorted, rounded to subangular, and cobble-sized clasts.

4.3.1. Age determination

Age determination of the studied section of the Seulimeum Formation is allowed by the presence of several biostratigraphically significant foraminifera index species for Neogene sediments (Fig. 10A–AJ). They are *Globigerinoides conglobatus*, *Globoturborotalita woodi*, *Globoquadrina dehiscens*, *Globorotalia humerosa*, *Globorotalia plesiotumida*, *Globorotalia pseudomiocenica*, and *Pulleniatina primalis*. From oldest to younger, local biozonation of the Seulimeum Formation could be defined as *Globorotalia humerosa - Globoquadrina dehiscens* zone, *Globoquadrina dehiscens - Globorotalia plesiotumida* zone, and *Globorotalia plesiotumida - Globoturborotalita woodi* zone. Based on this biozonation, the Seulimeum Formation is concluded to be deposited from Late Miocene to early Pleistocene, N17 to N21

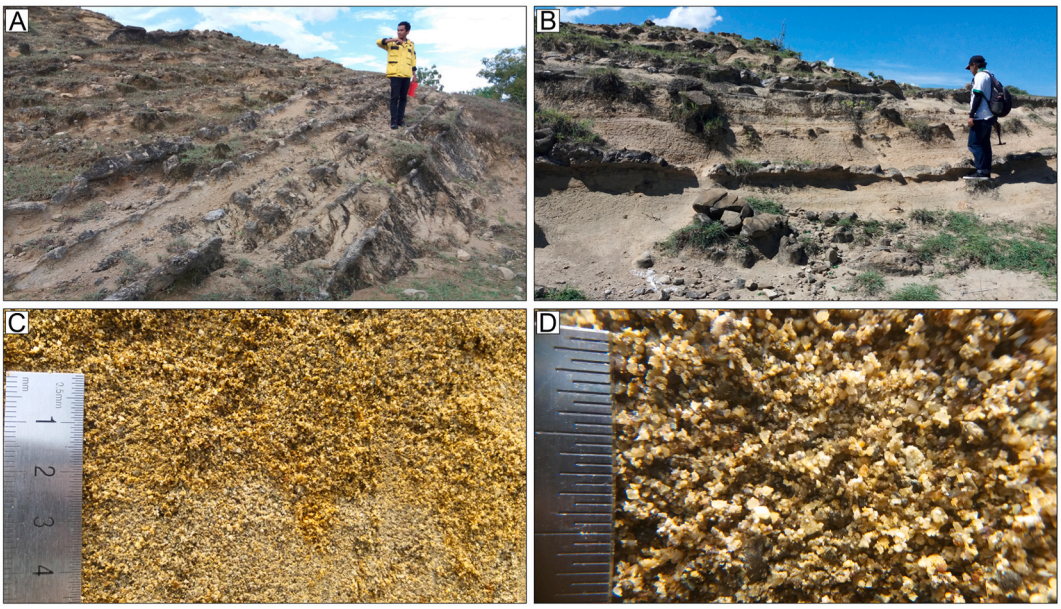

Fig. 7. Outcrop expression of facies F3 (people's height is ca. 169 cm long, a hammer is ca. 25 cm long): A, B) Thick-bedded sandstone intercalated with tuffaceous Sandstone with the thickness ranging from 30 cm to 3 m; C) Light brown to brown sandstone with medium to coarse grain size; D) Sandstone with quartz fragments, igneous rocks, and black minerals, with rounded to sub-angular shapes.

zone [26] or equivalent to M13b to PL6 zone of Wade et al. [27], ranging from about 8.6 to 2.3 Ma. The correlation of all the studied section based on biozonation is provided in Fig. 11, and their interpretation is explained as follow:

The *Globorotalia humerosa - Globoquadrina dehiscens* zone is defined by the first occurrence of *Globorotalia humerosa* at the base and the last occurrence of *Globoquadrina dehiscens* at the top of the zone. The first occurrence of *Globorotalia humerosa* are found at sample WK01 of Waduk Keuliling section and at sample TP02 of Tebing Putih section. This event are coincide with the first appearance of *Globorotalia plesiotumida* and *Globorotalia pseudomiocenica* at the base of N17 or M13b zone, which is about 8.6 Ma [26,27,52]. This biozonation was also marked by the first occurrence of *Pulleniatina primalis* (about 6.8 Ma; [27,52]) at sample JW01 (Seulimeum section) and BR01 (Beureunut River), and the first occurrence of *Globigerinoides conglobatus* (about 6.5 Ma; [27,52]) at sample RD01 of Reukih Dayah section. The last occurrence of *Globoquadrina dehiscens* (about 5.9 Ma; [27,52]) which marks the top of this zone, is found at sample WK03 of the Waduk Keuliling section.

In the middle part of the Seulimeum Formation ranging from about 5.9 to 3.8 Ma, are the *Globoquadrina dehiscens - Globorotalia plesiotumida* zone. It refers to the last occurrence of *Globoquadrina dehiscens* at its base and the last occurrence of *Globorotalia plesiotumida* at the top. The top of this zone is found at sample WK10, Waduk Keuliling section. The event of the last appearance of *Globorotalia plesiotumida* is about 3.8 Ma [27,52].

The *Globorotalia plesiotumida - Globoturborotalita woodi* zone, which ranges from about 3.8 to 2.3, is marked the upper part of the Seulimeum Formation. The last occurrence of *Globorotalia plesiotumida* divined the base of this zone, while the last appearance of *Globoturborotalita woodi* is noted at the top of this zone. The last occurrence of *Globoturborotalita woodi* is about 2.3 Ma [27,52] which is observed at sample WK12, Waduk Keuliling section.

4.3.2. Paleobathymetry

Based on benthonic foraminifera assemblage (Fig. 10), paleobathymetry of the Seulimeum Formation is assigned as deposited at the bathyal environment. Furthermore, the paleobathymetry of the Seulimeum Formation can be divided into an upper bathyal environment (200–1000 m water depth) and a lower bathyal environment (1000–4000 m water depth) (Fig. 12) [28–31]. Benthonic taxa typifying the upper bathyal include *Epistomina elegans*, *Lagenonodosaria scalaris*, *Quinqueloculina schwantzi*, *Spiroloculina corrugata*, *Streblus batavus*, *Nonion subturgidum*, *Trifarina bradyi*, *Astrononion fijiense*, *Cibicides grossepunctata*, *Lagena sulcata*, *Uvigerina bradyana*, *Bulimina pupoides*, *Siphonodosaria lepidula*, *Uvigerina aculeata*, *Bolivinita quadrilatera*, *Gyroidina neolodanii*, and *Karreriella bradyi* [53,54]. The lower bathyal taxa are represented by *Fursenkoina earlandi*, *Aphelophragmina semilineata*, *Bulimina rostratiformis*, *Saidovina carinata*, and *Bulimina subornata* [53,54].

Noteworthy is the presence of shelf benthonic assemblages as a mixture with bathyal microfaunas. This is interpreted as the result of downslope transport of the shelf sediment into the bathyal realm. In summary, the bathyal paleobathymetry interpretation based on foraminifera is in agreement with the deep marine depositional environment concluded from lithofacies analysis.

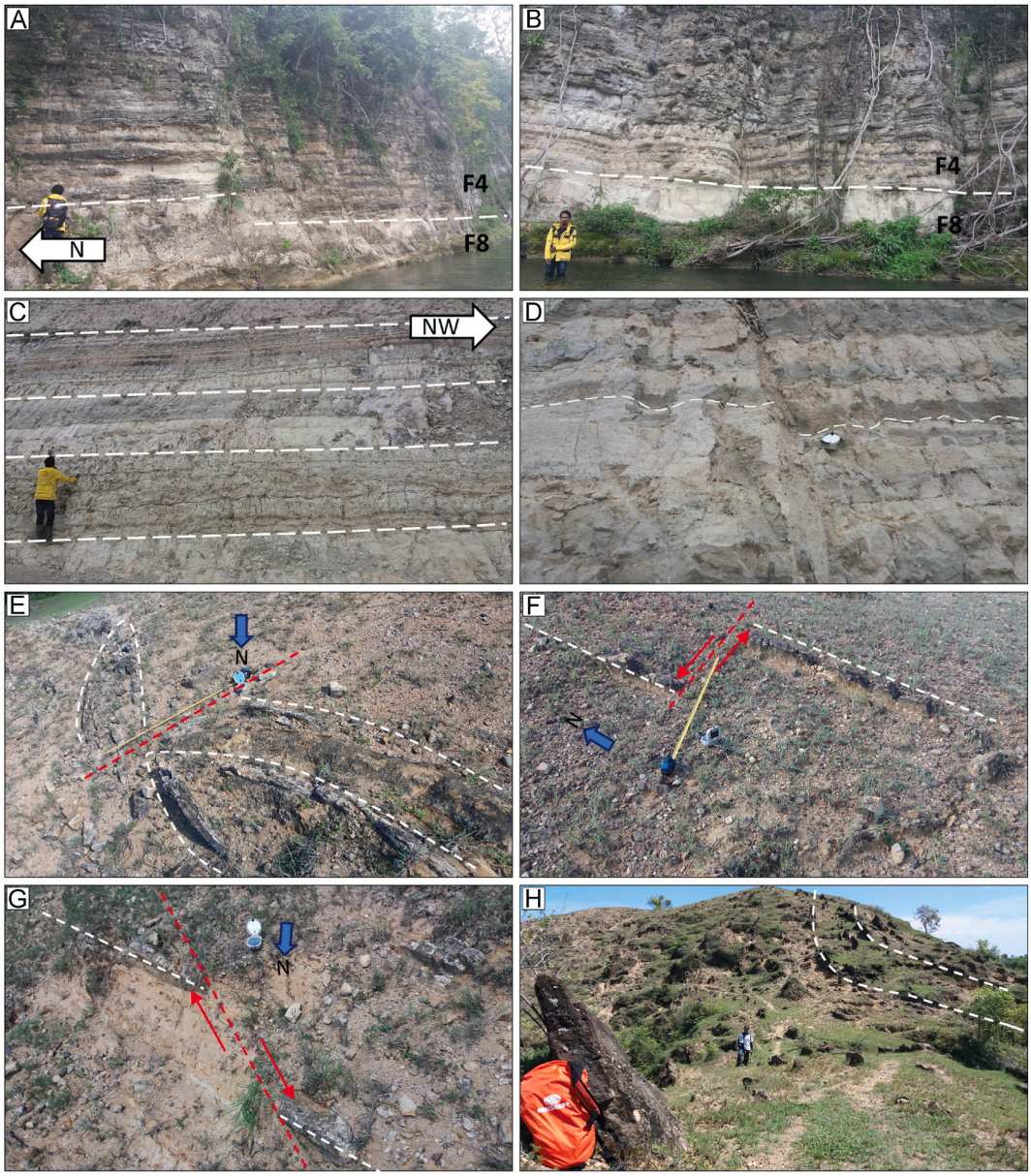

Fig. 8. Outcrop expression of facies F4, F5, and F8 (people's height is ca. 169 cm long), A, B) The sandy tuff facies (F8) overlying by succession of the sandstone to mudstone heterolithics facies (F4). C) Repetitions of the sandstone to mudstone heterolithics facies. D) Close up of the sandstone to mudstone heterolithics facies. E) The slumped sandstone facies (F5) shows the sandstone layer exhibits folding and faulting. F, G) The slumped sandstone facies (F5) shows displacement of the sandstone layer. H) Folding and irregularly oriented vertical layers in the upper right section of the photo.

4.4. Petrographic analysis

4.4.1. Texture and composition

The microscopic appearance of analyzed sandstone generally has fragments measuring from 0.05 to 1 mm or very fine-grained sand to coarse-grained sand based on the Udden-Wentworth grain scale. They have a degree of subangular to rounded, moderately sorted to poorly sorted. The inter-grain relationships that are often found in the incisions are dominant points and floating, but long contact inter-grain relationships can also be found in the samples. The sandstone of the Seulimeum Formation shows an immature textural maturity level, reflecting that the sediments have undergone close transport or have not experienced reworking.

The average composition of the sandstones of the Seulimeum Formation consists of 43% fragments, 41% matrix, 10% cement, and 6% porosity. The fragments composed of the minerals monocrystalline quartz (Qm), feldspars (F), polycrystalline quartz (Qp),

Fig. 9. Outcrop expression of facies F6 and F7 (hammer is ca. 25 cm long, pencil is ca. 15 cm long), (A & B) The siltstone facies (F6) with intercalation of cross to parallel laminated sandstones. C) Massive Siltstone; D) Siltstone layers contain large foram fossil remains. E, F) Massive claystone facies (F7).

sedimentary lithics (Ls), volcanic lithics (Lv), plutonic lithics (Lp), quartz in volcanic lithics (QLv), feldspars in volcanic lithics (FLv), chert (ch), heavy minerals (HM), amphiboles (Amp), mica muscovite (Ms), and fossils (Fs) (Fig. 13; Table 3). The matrix in the sandstones is composed of clay minerals as well as minerals that look like quartz. The description of each sandstone fragment is as follows.

4.4.2. Monocrystalline quartz (Qm)

Monocrystalline quartz (Qm) totaled 1952 grains or 19.9% of the total analyzed samples. Their size varies from 0.05 to 1 mm. The Qm grain with undulose extinction is not observed in the samples. Some of the monocrystalline quartz has overgrowth (growth as cement), while the others have inclusions of opaque minerals. This quartz appears to have a subrounded grain shape, and they do not seem to be in its ideal shape. This condition may be caused by abrasion when transported.

Table 2
Foraminifera distributions of studied sections.

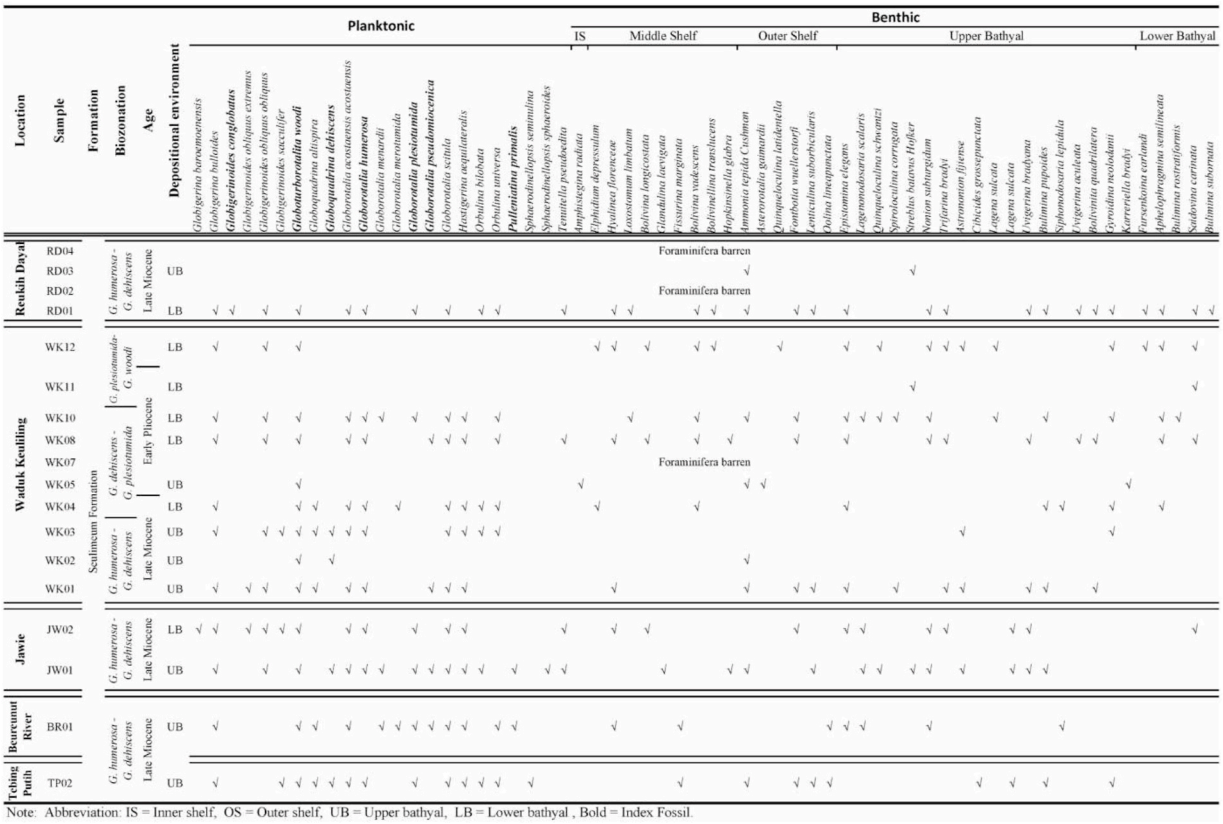

Note: Abbreviation: IS = Inner shelf, OS = Outer shelf, UB = Upper bathyal, LB = Lower bathyal , Bold = Index Fossil.

4.4.3. Polycrystalline quartz (Qp)

Polycrystalline quartz (Qp) totaled 86 grains or 1.1% of the total analyzed samples. They range in size from 0.05 to 1 mm. Polycrystalline quartz was generally composed of more than three types of quartz in one mineral grain (60%), but polycrystalline quartz, which only consisted of two to three quartz pieces, was also found in the samples (40%).

4.4.4. Plagioclase (P)

There were 292 plagioclase (P) grains, or 3.6%, observed from the total analyzed samples. The plagioclase has an average size of 0.5 mm with grain shapes from subrounded to rounded. They have a Carlsbad-albite twinning with a dark angle of 160–200 with a mineral refractive index greater than the refractive index of the balsam. Based on that, it can be concluded that the type of plagioclase is Andesine. Almost all of the plagioclase found was in relatively unfresh conditions/weathered.

4.4.5. Mica

The mica totaled 189 grains or 2.4% of the analyzed samples. The mica found in the sample is muscovite and biotite, ranging from about 0.1 to 0.2 mm. They are common as muscovite flakes or layers, which are slightly weathered and experience bending.

4.4.6. Sedimentary lithics (Ls)

The sedimentary lithics totaled 119 grains or 1.5% of the total analyzed samples. The sedimentary lithics have a size of about 0.4 mm–0.8 mm. It is dominated by sandstone which is composed of minerals such as quartz. A minor amount of chert is also observed.

4.4.7. Volcanic and plutonic lithics (Lv + Lp)

There were 258 lithic igneous rocks or 3.3% of the total samples tested. They have a size of about 0.1 mm–0.5 mm. The volcanic lithic dominates the igneous rocks lithic. In general, the volcanic lithic consists of andesite, while the plutonic lithic is composed of diorite.

Table 3 shows the compositional analysis of sandstone modal point counts. From this analysis, it can be seen that the fragments of Seulimeum Formation are composed of 19.9% monocrystalline quartz (Qm), 3.6% feldspars (F), 3.2% volcanic lithics (Lv), 2.4% mica

Fig. 10. Photomicrographs of selected planktonic foraminifera (A–G), Benthic foraminifera in lower bathyal (H–L), upper bathyal (M-AC), outer shelf (AD-AJ) depositional environment of the Seulimeum Formation: A) *Globoturborotalita woodi,* B) *Globorotalia humerosa,* C) *Globorotalia plesiotumida,* D) *Globorotalia pseudomiocenica,* E) *Pulleniatina primalis,* F) *Globigerinoides conglobatus,* G) *Globoquadrina dehiscens.* H) *Fursenkoina earlandi,* I) *Aphelophragmina semilineata,* J) *Bulimina rostratiformis,* K) *Saidovina carinata,* L) *Bulimina subornata,* M) *Epistomina elegans,* N) *Lagenonodosaria scalaris,* O) *Quinqueloculina schwantzi, P) Spiroloculina corrugata, Q) Streblus batavus, R) Nonion subturgidum,* S) *Trifarina bradyi,* T) *Astrononion fijiense,* U) *Cibicides grossepunctata,* V) *Lagena sulcata,* W) *Uvigerina bradyana,* X) *Bulimina pupoides,* Y) *Siphonodosaria lepidula,* Z) *Uvigerina aculeata,* AA) *Bolivinita quadrilatera,* AB) *Gyroidina neolodanii,* AC) *Karreriella bradyi,* AD) *Ammonia tepida cushman,* AE) *Ammonia tepida,* AF) *Asterorotalia gaimardii,* AG) *Quinqueloculina latidentella,* AH) *Fontbotia wuellerstorfi,* AI) *Lenticulina suborbicularis,* AJ) *Oolina lineapunctata.*

muscovite (Ms), 1.7% heavy mineral, 1.5% sedimentary lithics (Ls), 1.1% polycrystalline quartz (Qp), 1.1% amphibole, 0.8% fossil, 0.6% feldspars in volcanic lithics, 0.2% quartz in volcanic lithics, 0.2% chert, and 0.1% plutonic lithics. Furthermore, the sandstone compositional data are grouped into Qt, F, L, Qm, and Lt for sandstone classification and provenance analysis.

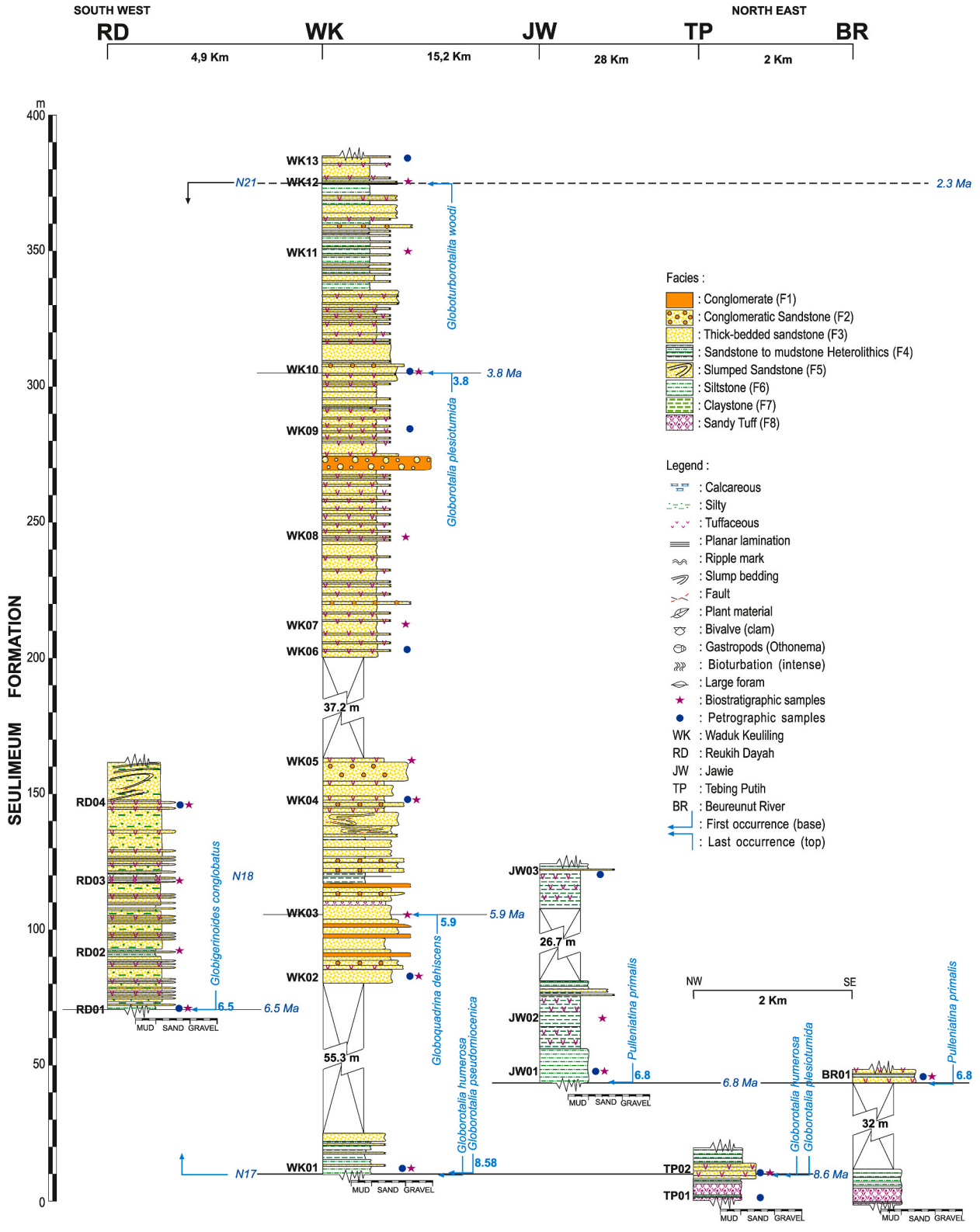

Fig. 11. Stratigraphic correlation of the five studied locations (Reukih Dayah, Waduk Keuliling, Jawie, Tebing Putih, and Beureunut River).

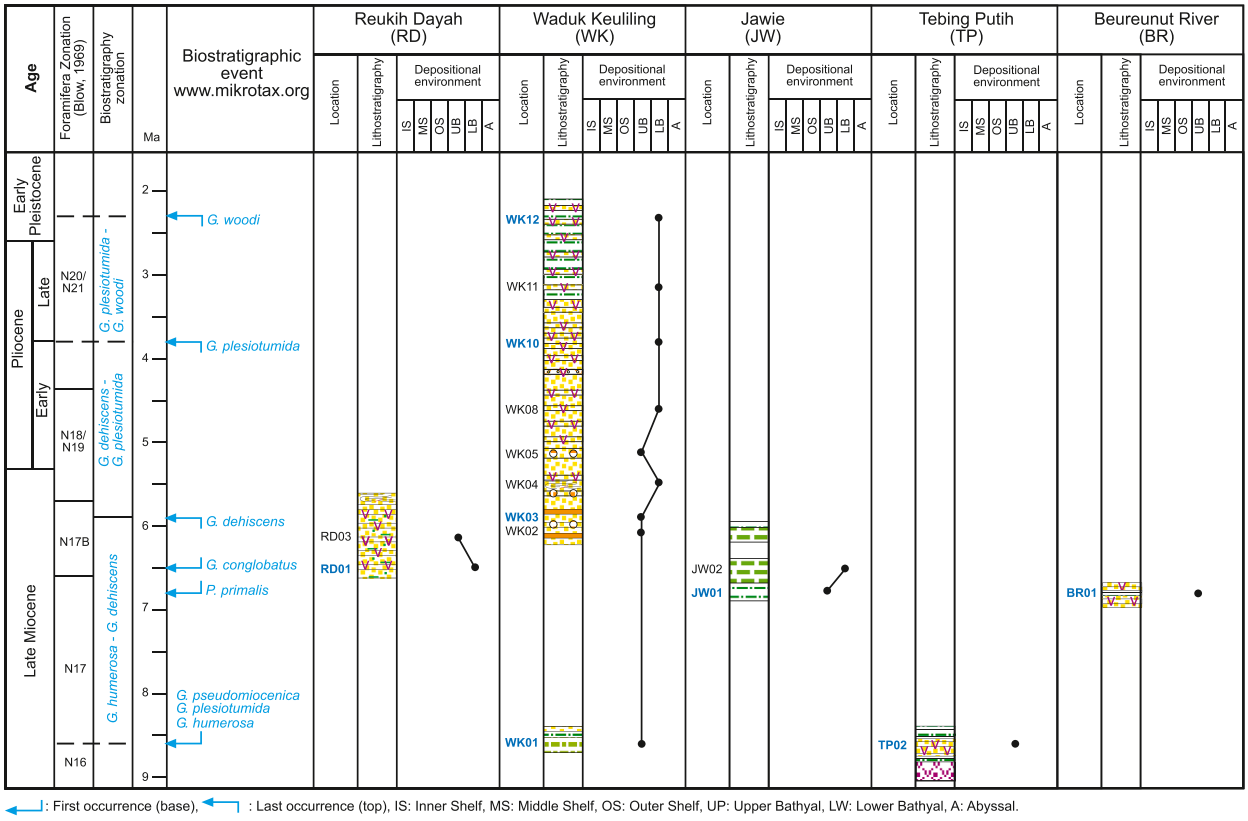

Fig. 12. The depositional environment of the studied section of the Seulimeum Formation.

4.5. Sandstone classification

The classification of the sandstones is based on Pettijohn [39], and Garzanti [40], which uses total quartz, feldspar, lithic, and matrix components as the basis for its classification. The total quartz (Q), feldspars (F), and rock fragments (R) components in these rocks were then plotted on the Q-F-R diagram of Pettijohn [39], as shown in Fig. 14A. Based on this diagram, the sandstone of the Seulimeum Formation is included as subarkose, sublithic arenite, and lithic arenite. Using the triangular quartz (Q), feldspars (F), and lithics (L) diagram of Garzanti [40] sandstone classification, the sandstone of the Seulimeum Formation is classified as litho-quartzose, feldspatho-litho-quartzose, and litho-feldspatho-quartzose (Fig. 14B).

4.6. Provenance

The constituent material of sandstone can come from the remnants of erosion from igneous rock, volcanic rock, and metamorphic rock, or it can also come from pre-existing sedimentary rock. Each of these rocks was formed in different processes and conditions. Differences in processes and conditions cause differences in mineral composition and the proportions of each mineral in each rock type. In other words, the results of erosion from igneous rocks will consist of proportions and composition of minerals that differ from the results of erosion from metamorphic rocks.

The composition of the Seulimeum Formation sandstones suggests that the main source areas are igneous, sedimentary, and metamorphic rocks. The results of the quartz composition, as shown in Table 3, show that the quartz composition is dominated by monocrystalline quartz with a percentage of 19.9%. All the monocrystalline quartz present in the observed samples has a uniform extinction (non-undulatory extinction). According to Tucker [55] and Basu et al. [56], monocrystalline quartz, which has many non-undulatory extinction properties, generally originates from plutonic igneous rocks. This also indicates that the sandstone of the Seulimeum Formation has not undergone high-level metamorphism, which can change the quartz to undulatory extinction. The polycrystalline quartz is only present in the amount of around 1.1%. The minor presence of polycrystalline quartz may be due to the mineral properties of polycrystalline quartz, which are not as resistant as the monocrystalline quartz, or it can also suggest that the sandstone of Seulimeum Formation has not experienced reworking [56,57]. Polycrystalline quartz has generally been exposed to forces that cause quartz to deform and split into several pieces. Individual parts of quartz can become weak zones making them more susceptible to weathering and abrasion during transport.

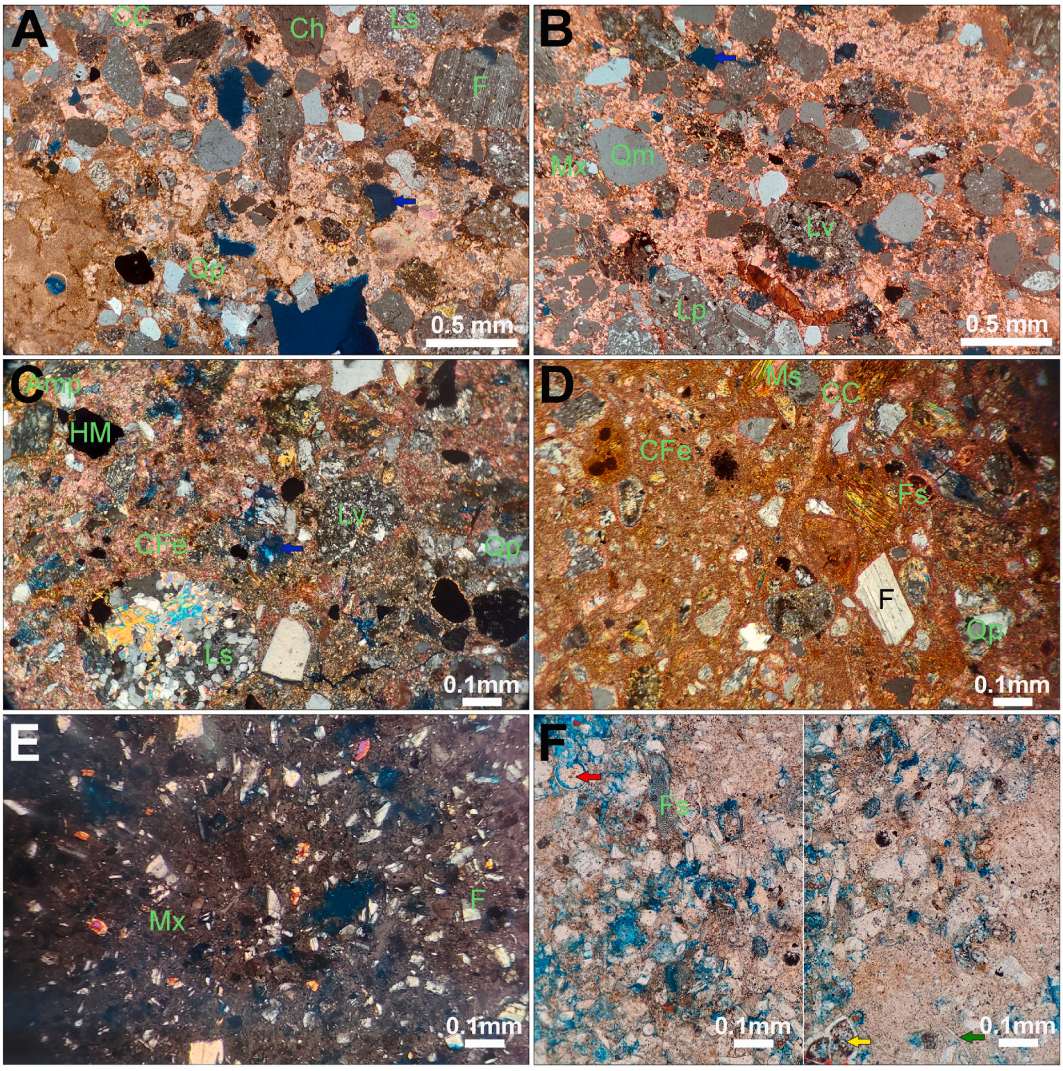

Fig. 13. Photomicrographs of thin sections of Sandstone (A–D), sandy tuff (E), and tuffaceous Sandstone (F) from the Seulimeum Formation (Monocrystalline quartz (Qm), feldspars (F), polycrystalline quartz (Qp), sedimentary lithics (Ls), volcanic lithics (Lv), plutonic lithics (Lp), carbonate cement (CC), Fe oxide cement (CFe), Matrix (Mx), chert (ch), heavy mineral (HM), amphibole (Amp), muscovite mica (Ms), fossils (Fs), intergranular porosity (blue arrows), silica cementation commonly found on fossil shells (red arrows), Fe-oxide cementation that may replace silica cementation on shells (yellow arrows), and volcanic glass present in small amounts (green arrows).

The analysis of the sandstone modal point counts also shows that both K-feldspar and plagioclase can be found in the samples of the Seulimeum Formation, with a total of 3.6%. K-feldspar is commonly found in acid igneous rocks and metamorphic rocks such as gneiss [58]. In addition, K-feldspar can also come from a rework of sedimentary rocks such as arkose sandstones [59]. Plagioclase is a mineral often found in volcanic igneous rocks, acidic to alkaline igneous rocks, and can also be derived from metamorphic rocks derived from sedimentary rock protolith. The plagioclase from each rock has characteristics that make it different from plagioclase from other rocks, such as zoning on plagioclase from volcanic rocks, high albite composition in acid igneous rocks, and high anorthite from alkaline igneous rocks.

Based on the twinning measurements the plagioclase, the analyzed sample consists of Andensine. The andesine has an albite composition of about 50–70% which indicates that the plagioclase can originate from intermediate to acid igneous rocks such as andesite, diorite, trachyte, syenite, rhyolite, and granite but can also originate from metamorphic rocks. The total proportion of plagioclase that comes from the intermediate rocks such as andesite and diorite should be very abundant, but in the analyzed samples, the observed plagioclase is only around 3.6%. Likewise, if plagioclase originates from acid igneous rocks, it should be followed by abundant k-feldspar minerals. However, the presence of k-feldspar is very small. Therefore, plagioclase likely originates from low to intermediate metamorphic rocks such as schist and phyllite, where plagioclase can form under metamorphic conditions at temperatures of 800°–900 °C. The metamorphic rocks origin is also shown by the lack of zoning in the plagioclase of the analyzed samples [60].

Table 3
Sandstone modal point counts.

Sample	Qm	F	Qp	Ls	Lv	Lp	Lm	QLv	FLv	CC	Cfe	Mx.	ch	HM	Pore	UR	Amp	Ms	Fs
WK13	187	29	6	12	19	0	0	0	0	83	43	440	0	12	57	3	47	49	12
WK10	200	36	7	13	32	0	0	0	0	28	88	516	0	10	45	4	0	21	0
WK09	279	118	1	1	74	1	0	0	43	12	31	193	4	64	101	5	11	62	0
WK06	148	19	10	8	25	0	0	0	0	75	22	583	0	0	73	13	4	10	10
WK04	88	4	7	41	11	0	0	0	0	47	16	693	0	0	76	17	0	0	0
WK02	185	13	6	14	24	0	0	0	0	89	61	257	1	21	212	0	27	48	41
RD04	257	63	30	11	42	1	0	12	2	125	21	331	0	11	72	22	0	0	0
RD01	250	9	19	20	26	2	0	0	3	65	32	237	9	16	304	10	0	0	0

Note: Monocrystalline quartz (Qm), feldspars (F), polycrystalline quartz (Qp), sedimentary lithics (Ls), volcanic lithics (Lv), plutonic lithics (Lp), metamorphic lithics (Lm), quartz in volcanic lithics (QLv), feldspars in volcanic lithics (FLv), carbonate cement (CC), Fe oxide cement (CFe), Matrix (Mx), chert (ch), heavy mineral (HM), pore, unrecognized (UR), amphibole (Amp), Mika muscovite (Ms), and fossil (Fs).

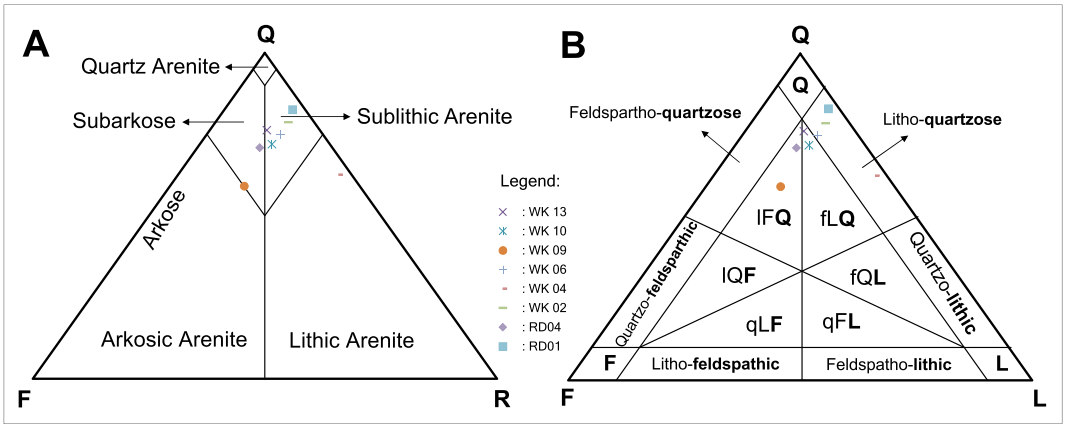

Fig. 14. Fragment composition of the Seulimeum Formation plotted in the Q-F-R (A) and Q-F-L ternary classification (B) [39,40]. **Q** = quartz, quartzose, **F** = feldspar, feldspathic, R = rock fragments, **L** = lithic, l**F**Q = litho-feldspatho-quartzose, l**Q**F = litho-quartzo-feldspathic, q**L**F = quartzo-litho-feldspathic, q**F**L = quartzo-feldspatho-lithic, f**Q**L = feldspatho-quartzo- lithic, and f**L**Q = feldspatho-litho-quartzose.

The results of the petrographic analysis show the presence of fragments in the form of sedimentary lithic, volcanic lithic, and plutonic lithic. This indicates that the source rocks of the Seulimeum Formation may originate from sedimentary and igneous rocks. The sedimentary lithic fragments found in the sample also indicate that before the Seulimeum Formation was deposited, older sedimentary rocks had been formed in the basin. The petrographic analysis also exhibits that the mica found in the samples is muscovite and biotite. These minerals are commonly found in igneous rocks but are especially abundant in metamorphic rocks such as schist [61].

4.7. Tectonic setting

The interpretation of the tectonic setting during the deposition of the Seulimeum Formation using the method of Dickinson [42] and Dickinson et al. [43]. The plotting of Qt-F-L and Qm-F-Lt composition in the triangular diagram suggests that all the sandstone samples of the Seulimeum Formation accumulated in the recycled orogen or the quartzose recycled tectonic setting (Fig. 15A and B).

The recycled orogen type is a vast complex with three areas that can become source rock: the subduction zone, which has experienced an uplift; the suture zone around the collision; and the foreland uplift associated with the fold-thrust belt [42]. The fold-thrust belt can exist in two different tectonic settings associated with collision zones or arc orogens. These three places may be present simultaneously because non-parallel subduction zones cause them, so one part has experienced a collision while the other is still in a state of subduction. Furthermore, to differentiate in what part of the recycled orogen zone the sediments accumulated, can use the Qp-Lv-Ls triangular diagram [62]. The results of the fragments composition plot on the Qp-Lv-Ls diagram show that the origin of the sandstones of the Seulimeum Formation is from the arc orogen sources (Fig. 15C). Additionally, the occurrence of tuff facies in the Seulimeum Formation suggests that the deposition of this formation were related to magmatic arc provinces.

4.8. Discussion on the late Neogene basin forming and its depositional system

The oldest rocks in the study area are from the late Mesozoic, known as the Woyla Nappe (Woyla Group and Bentaro Volcanic Rocks), which represent the basement rocks [6,63]. During the emplacement of Woyla in the late mid-Cretaceous, Sumatra was exposed to subaerial erosion, but no late Cretaceous to early Palaeogene sediments were recognized in situ. However, volcanic activity occurred during this time, which in the study area is represented by Granodiorite to diorite intrusives [6,63].

In the middle to late Eocene, there were widespread extensions in Sundaland, including Sumatra and the study area [13]. The formation of hosts and grabens, which resulted in stratigraphic development, began in the late Eocene to early Oligocene. Sedimentation in the graben results from local horst erosion, which in the study area is represented by the deposition of the Meucampli Formation in a paralic to the fluviatile environment. During the late Oligocene, the Barisan Mountains are starting to develop as the main structural element due to a change in the regional tectonic regime. However, the mountain range is still restricted in extent and height [14].

Extension in the early to middle Miocene is limited in the southwest part of the subduction part of Sundaland [13], also marking the beginning of transgression, which reached its peak in the middle Miocene [14]. During this time, in the study area, the Peunasu Formation was deposited in a fluvial-paralic to open marine setting [6]. Volcanic activity was also recorded in the early Miocene by Breueh Volcanic dan Bentaro Volcanic Rocks [6,12]. A sedimentary rock accumulated in the middle Miocene, known as Padang Tiji Members, was deposited in an open marine environment [6].

The compression phase in the late Miocene is marked by the development of a widespread fold and thrust belt around the margin of Sundaland [13]. The study area during this time was in the back-arc basin setting where the studied Seulimeum Formation was deposited. The depositional model of the late Neogene Seulimeum Formation in the back-arc basin illustrating its relation with their sediment source and the development of the GSF zone is displayed in Fig. 16 and discussed below.

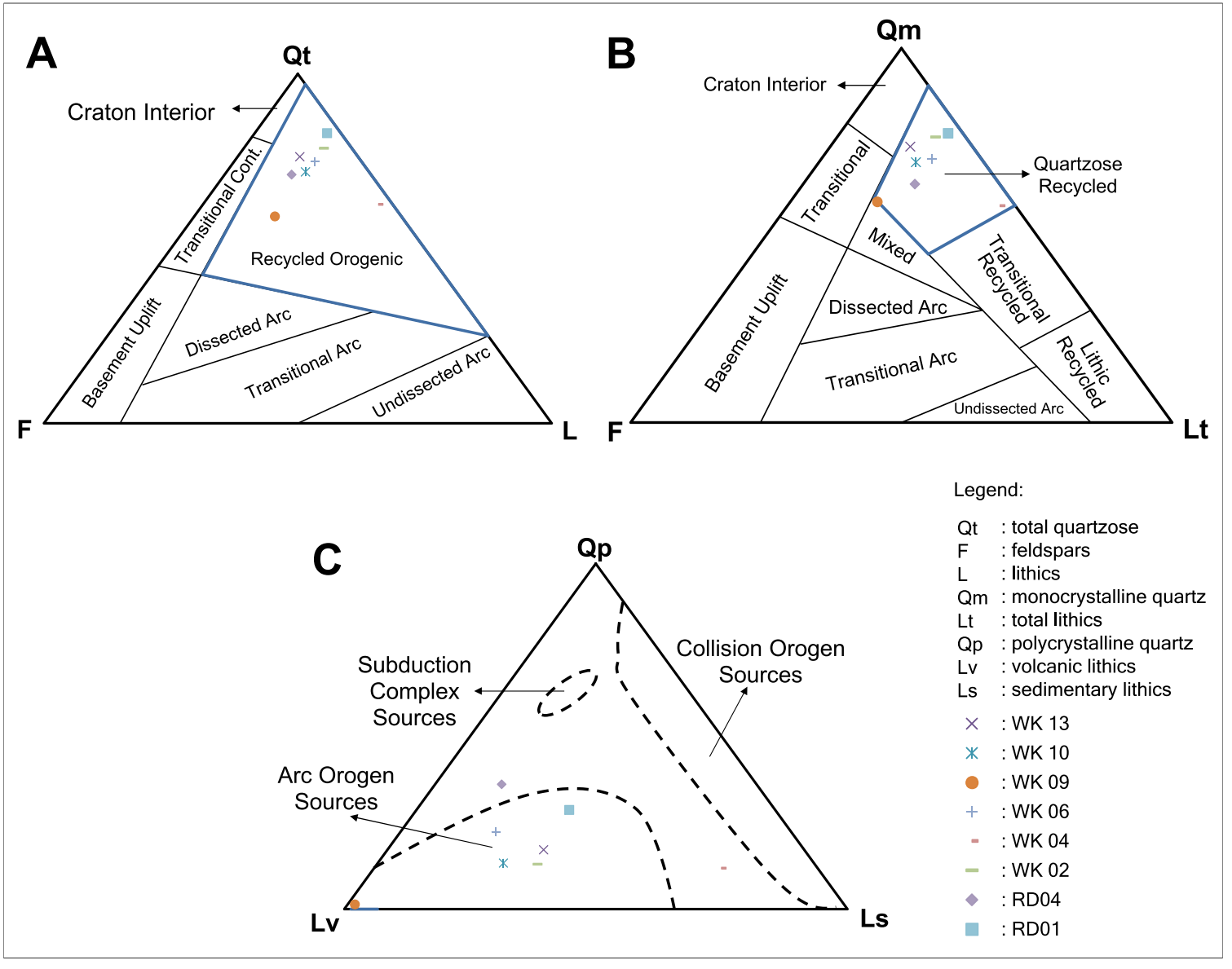

Fig. 15. Provenance ternary Qt-F-L (A), Qm-F-Lt (B), and Qp-Lv-Ls (C) plots of the sandstones of Seulimeum Formation [42,43,62]. Qt = Qm + Qp, L = Lv + Ls, and Lt = L + Qp.

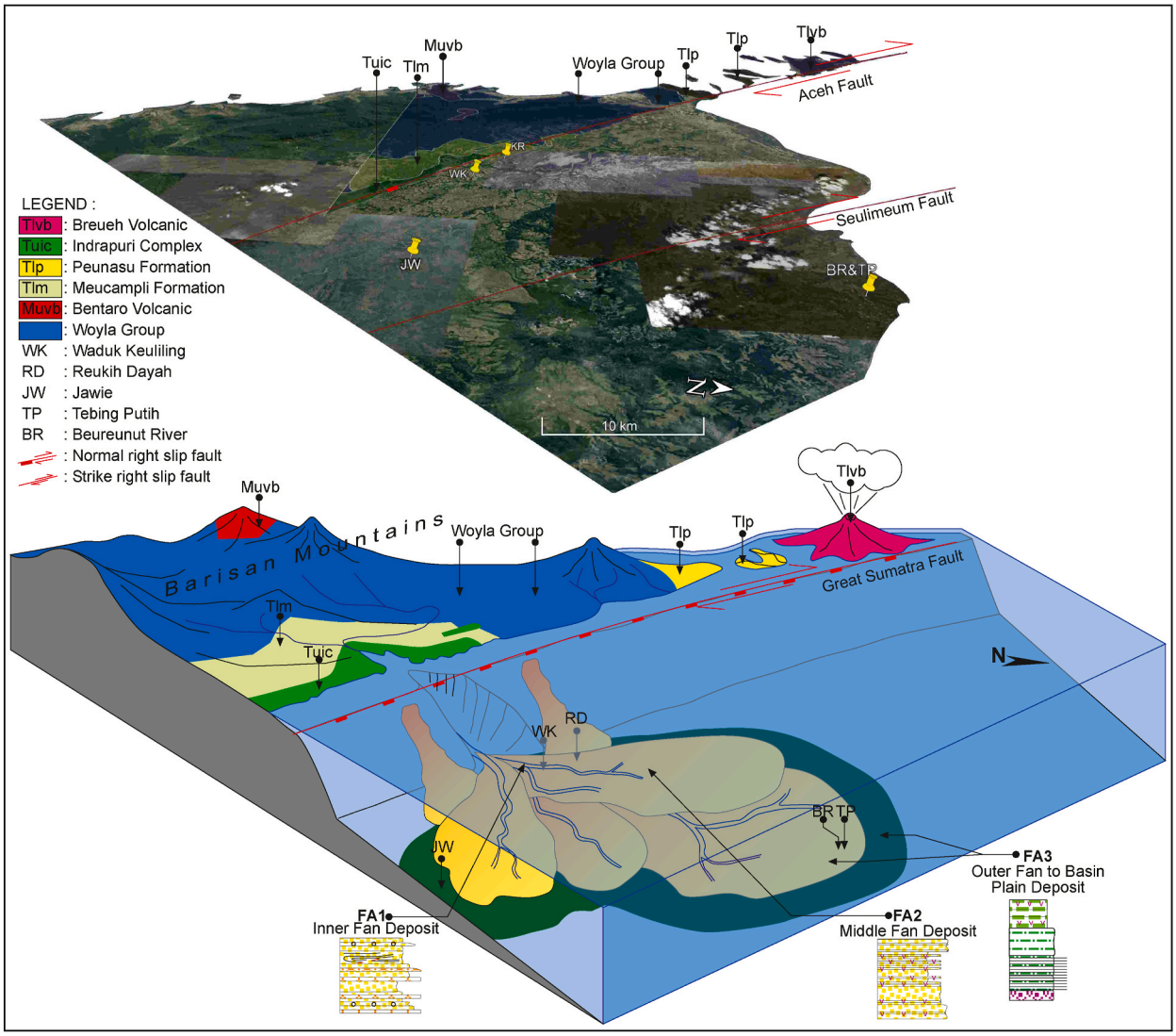

Fig. 16. Depositional model of Seulimeum Formation showing facies association in the deep-marine environment. The east-north-east part of the Great Sumatran Fault zone is the hanging wall part forming the accommodation space for the deposition of the sediments. The west-south-west part of the Great Sumatran Fault is the footwall part, which becomes the main high area of the sedimentary source material (modified from Refs. [6, 17,64]).

Based on the lithofacies analysis, the Seulimeum Formation can be specified as three facies association of a deep-marine depositional system [17–19,47]. It consists of inner fan deposit (FA1), middle fan deposit (FA2), and outer fan to basin plain deposit (FA3). Furthermore, it is interpreted that the development of the GSF controls the formation of this deep-marine depositional setting. The GSF is a dextral slip fault [1,12,65,66] which most probably its movement was relatively normal right-slip fault. During late Neogene, the east-north-east part of the GSF zone is the hanging wall part forming the accommodation space for the deposition of the Seulimeum Formation. This newly formed basin, named the Breueh Basin [1], is located above the previous larger basin known as Northwest Aceh Basin [6,66]. In the late Neogene time, their paleobathymetry shown by foraminifera analysis are in bathyal environment.

The weak zone of the GSF becomes the slope and canyon, which is evidenced by the presence of an inner fan deposit (FA1) near the fault (Reukih Dayah and Waduk Keuliling location). While further from the slope, the Jawie location is dominated by a suspension deposit (outer fan to basin plain deposit, FA3). The Tebing Putih and Beureunut River locations located further north from the slope/fault zone are also characterized by fine-grained sediment of middle fan deposit (FA2) and outer fan to basin plain deposit (FA3). These two locations are located closer to the Miocene volcanic activity (Breueh Volcanic), resulting in a more dominant thick tuff layer in their stratigraphic succession.

Moreover, the west-south-west part of the GSF (the Barisan Mountains) is suggested as the footwall part, which becomes the main high area of weathering and erosion of the sedimentary source material of the Seulimeum Formation. It is concluded that the sediment

source is dominated by the Woyla Group, with some contributions from Bentaro volcanic and Paleogene to early Neogene sediments, as shown by the provenance analysis.

Based on the foraminifera analysis, the oldest biozonation of the Seulimeum Formation is the *Globorotalia humerosa - Globoquadrina dehiscens* zone which is ranging from 8.6 to 5.9 Ma. This age range are suggested as the age of the beginning of the Breueh Basin forming due to commencement of the GSF. Therefore, it is inferred that the initiation of GSF in northwestern Sumatra are in the late Miocene, not older than 8.6 Ma and not younger than 5.9 Ma. This result is in contrast with the earliest opinion about the time of the initiation of the GSF by Barber & Crow [3] and Ghosal et al. [1] (Middle Miocene) and by Sieh and Natawidjaja [2] and Curray [5] (Pliocene). This difference is probably caused by the lack of age control of the oldest oceanic crust in the Andaman Sea spreading system which is tought to be related with initiation of the GSF [67].

Moreover, the initiation of GSF in the late Neogene time also resulted in the further growth and re-emergence of the Barisan Mountains rather than their first occurrence in the late Oligocene [4]. The major sediment influx from the mountains into the backarc basins of Sumatra is following this event. The Barisan Mountains range in the late Neogene time became an important source of sediments. Morton et al. [68] reported that in the middle Miocene, there was a major change in the source of clastic sediments in the North Sumatra Basin from a granitic terrain Asahan Arch and the Malay Peninsula (to the east or SE) to the area of the Barisan Mountains (to the west or SW). From the late Miocene onwards, the turbiditic formations become an increasing component in the deep water sediment throughout the backarc basins of Sumatra. In the North Sumatra Basin, these rock units are known as the Seumpo, the Upper Baong, and Keutapang Formations [69]. They also acknowledge in the Central Sumatra Basin as the Binio and Lower Petani Formations [70,71], while in the South Sumatra Basin as the Airbenakat Formation [72]. In the research area, these late Neogene turbiditic units are now proposed to be represented by the Seulimeum Formation.

5. Conclusions

Seulimum Formation is characterized by eight lithofacies, including conglomerate (F1), conglomeratic sandstone (F2), thick-bedded sandstone (F3), sandstone to mudstone heterolithics (F4), slumped sandstone (F5), siltstone (F6), claystone (F7), and sandy tuff (F8). It can be grouped into three facies associations, which are inner fan deposit (FA1), middle fan deposit (FA2), and outer fan to basin plain deposit (FA3), found in the deep-water depositional setting.

The local biozonation of the Seulimeum Formation, from oldest to younger, defined as *Globorotalia humerosa - Globoquadrina dehiscens* zone, *Globoquadrina dehiscens - Globorotalia plesiotumida* zone, and *Globorotalia plesiotumida - Globoturborotalita woodi* zone. Based on this biozonation, the studied section is concluded to be deposited from the late Miocene to the early Pleistocene (N17 to N21), ranging from about 8.6 to 2.3 Ma. The paleobathymetry is in the bathyal environment.

The sandstone of the Seulimeum Formation is included as subarkose, sublithic arenite, and lithic arenite. They originate from various igneous, sedimentary, and metamorphic rocks from arc orogen sources. During the late Neogene, the depositional site was controlled by the development of the GSF zone, which is thought to have a relatively normal right-slip fault allowing the formation of deep-marine accommodation space in the east-north-east part of the fault. At the same time, the Barisan Mountains, as the footwall part (west-south-west part of the fault) is considered as the main high area for supplying the sedimentary source material. The provenance of the Seulimeum Formation is comprised mainly of the Woyla Group, with some contributions from Bentaro volcanic and Paleogene to early Neogene sediments.

Furthermore, it is inferred from the findings that the initiation of the GSF, which is concurrent with the uplift of the Barisan Mountains in the northern domain of Sumatra, occurred in the range of 8.6–5.9 Ma (late Miocene).

Author contribution statement

Gartika Setiya Nugraha: Conceived and designed the experiments; Performed the experiments; Analyzed and interpreted the data; Contributed reagents, materials, analysis tools or data; Wrote the paper.

Edy Sunardi; Iyan Haryanto; Billy Gumelar Adhiperdana and Rakhmat Fakhruddin: Conceived and designed the experiments; Analyzed and interpreted the data; Wrote the paper.

Ria Fitriany and Dina Gunarsih: Contributed reagents, materials, analysis tools or data.

Data availability statement

Data associated with this study has been deposited at Geological Engineering, Faculty of Engineering, Universitas Syiah Kuala, Banda Aceh 23111, Indonesia.

Declaration of competing interest

The authors declare that they have no known competing financial interests or personal relationships that could have appeared to influence the work reported in this paper.

Acknowledgments

The first author is grateful to Badan Pengembangan Sumber Daya Manusia (BPSDM) Aceh Indonesia for the educational funding assistance. The research was undertaken with financial support by Kementerian Riset, Teknologi, dan Pendidikan Tinggi (Ristekdikti), and Lembaga Pengelola Dana Pendidikan (LPDP) Indonesia. The author is also indebted to all the field and laboratory teams who have assisted in implementing this research. The author thank the journal editor and two anonymous reviewers for their constructive comments and suggestions that greatly improved the original manuscript.

References

[1] D. Ghosal, S.C. Singh, A.P.S. Chauhan, N.D. Hananto, New insights on the offshore extension of the Great Sumatran fault, NW Sumatra, from marine geophysical studies, Geochemistry, Geophys. Geosystems. 13 (2012) 1–18, https://doi.org/10.1029/2012GC004122.
[2] K. Sieh, D. Natawidjaja, Neotectonics of the Sumatran Fault, Indonesia, J. Geophys. Res. Solid Earth 105 (B12) (2000) 28295–28326, https://doi.org/10.1029/2000jb900120.
[3] A.J. Barber, M.J. Crow, Chapter 13 Structure and structural history, Geol. Soc. London, Mem 31 (2005) 175–233, https://doi.org/10.1144/GSL.MEM.2005.031.01.13.
[4] M.E.M. De Smet, A.J. Barber, Chapter 7 tertiary stratigraphy, Geol. Soc. London, Mem 31 (2005) 86–97, https://doi.org/10.1144/GSL.MEM.2005.031.01.07.
[5] J.R. Curray, Tectonics and history of the Andaman Sea region, J. Asian Earth Sci. 25 (2005) 187–232, https://doi.org/10.1016/j.jseaes.2004.09.001.
[6] J.D. Bennett, D.M. Bridge, N.R. Cameron, A. Djunuddin, S.A. Ghazali, D.H. Jeffery, W. Kartawa, W. Keats, N.M.S. Rock, S.J. Thompson, R. Whandoyo, Geologic Map of the Banda Aceh Quadrangle, 1981. North Sumatra.
[7] J. Clure, Chapter 10 Fuel resources: oil and gas, Geol. Soc. London, Mem 31 (2005) 131–141, https://doi.org/10.1144/GSL.MEM.2005.031.01.10.
[8] H. Doust, R.A. Noble, Petroleum systems of Indonesia, Mar. Petrol. Geol. 25 (2008) 103–129, https://doi.org/10.1016/j.marpetgeo.2007.05.007.
[9] R.J. Hwang, T. Heidrick, B. Mertani, Qivayanti, M. Li, Correlation and migration studies of north central Sumatra oils, Org. Geochem. 33 (2002) 1361–1379, https://doi.org/10.1016/S0146-6380(02)00104-3.
[10] P. Lunt, Partitioned transtensional cenozoic stratigraphic development of North Sumatra, Mar. Petrol. Geol. 106 (2019) 1–16, https://doi.org/10.1016/j.marpetgeo.2019.04.031.
[11] L.D. Meckel, Exploring a 19th century Basin in the 21st century : seeing the North Sumatra Basin with new eyes, Proc. 36th AAPG Int. Conf. Exhib. Singapore. 10464 (2012) 1–65.
[12] Y.M. Lai, S.L. Chung, A.A. Ghani, S. Murtadha, H.Y. Lee, M.F. Chu, Mid-Miocene volcanic migration in the Mid-Miocene volcanic migration in westernmost Sunda arc induced by India-Eurasia collision, Geol. Geol. Soc. Am. 49 (2021) 713–717, https://doi.org/10.1130/G48568.1.
[13] M. Pubellier, C.K. Morley, The basins of Sundaland (SE Asia): evolution and boundary conditions, Mar. Petrol. Geol. 58 (2014) 555–578, https://doi.org/10.1016/j.marpetgeo.2013.11.019.
[14] A.J. Barber, M.J. Crow, M.E.M. De Smet, Chapter 14 tectonic evolution, Geol. Soc. London, Mem 31 (2005) 234–259, https://doi.org/10.1144/GSL.MEM.2005.031.01.14.
[15] R. Anderton, Geological Society , London , Special Publications Clastic facies models and facies analysis Clastic facies models and facies analysis, Geol. Soc. London, Spec. Publ. 18 (1985) 37–47, https://doi.org/10.1144/GSL.SP.1985.018.01.03.
[16] R.W. Dalrymple, Interpreting sedimentary successions: facies, facies analysis and facies models, in: N.P. James, R.W. Dalrymple (Eds.), Facies Models 4, Library and Archives Canada Cataloguing, Geological Association of Canada, 2010.
[17] G. Nichols, Sedimentology and Stratigraphy, second ed., Wiley Blackwell, United Kingdom, 2009.
[18] H.W. Posamentier, R.G. Walker, Facies Models Revisited, 2006.
[19] G. Shanmugam, Slumps Slides, Debris Flows, Turbidity Currents, and Bottom Currents: Implications ☆, Elsevier Inc., 2013 https://doi.org/10.1016/b978-0-12-409548-9.04380-3.
[20] P.J. Talling, G. Malgesini, E.J. Sumner, L.A. Amy, F. Felletti, G. Blackbourn, C. Nutt, C. Wilcox, I.C. Harding, S. Akbari, V. Mangiagalli, Planform Geometry , Stacking Pattern , and Extrabasinal Origin of Low Strength and Intermediate Strength Cohesive Debris Fl Ow Deposits in the Marnoso-Arenacea Formation, 2012, pp. 1207–1230, https://doi.org/10.1130/GES00734.1. Italy.
[21] P.J. Talling, D.G.M. Asson, E.J. Sumner, Subaqueous sediment density flows : depositional processes and deposit types, Sedimentology 59 (2012) 1937, https://doi.org/10.1111/j.1365-3091.2012.01353.x. –2003.
[22] I.A. Kane, B.C. Kneller, M. Dykstra, A. Kassem, W.D. Mccaffrey, Anatomy of a Submarine Channel – Levee : an Example from Upper Cretaceous Slope Sediments, vol. 24, Rosario Formation , Baja California, Mexico, 2007, pp. 540–563, https://doi.org/10.1016/j.marpetgeo.2007.01.003.
[23] C. Botziolis, A.G. Maravelis, G. Pantopoulos, S. Kostopoulou, O. Catuneanu, A. Zelilidis, Stratigraphic and paleogeographic development of a deep-marine foredeep : central Pindos foreland basin , western Greece, Mar. Petrol. Geol. 128 (2021), 105012, https://doi.org/10.1016/j.marpetgeo.2021.105012.
[24] R. Fakhruddin, Biostratigraphy and depositional environment of early to middle Miocene Sediments at Kulon Progo, Wonosari, and Punung areas based on their foraminiferal and palynological assemblages, Indones. J. Geosci. 6 (2019) 73–101, https://doi.org/10.17014/ijog.6.1.73-101.
[25] A. Maravelis, A. Zelilidis, Paleoclimatology and paleoecology across the eocene/Oligocene boundary , thrace basin , northeast aegean Sea , Greece, Palaeogeogr. Palaeoclimatol. Palaeoecol. 365–366 (2012) 81–98, https://doi.org/10.1016/j.palaeo.2012.09.015.
[26] W.H. Blow, in: Proc 1st (Ed.), Late Middle Eocene to Recent Planktonic Foraminiferal Biostratigraph, vol. 1, Int. Conf. Planktonic Microfossils, Geneva, 1969, pp. 199–422.
[27] B.S. Wade, P.N. Pearson, W.A. Berggren, H. Pälike, Review and revision of Cenozoic tropical planktonic foraminiferal biostratigraphy and calibration to the geomagnetic polarity and astronomical time scale, Earth Sci. Rev. 104 (2011) 111–142, https://doi.org/10.1016/j.earscirev.2010.09.003.
[28] W.A. Berggren, Recent advances in Cenozoic planktonic foraminiferal biostratigraphy, biochronology, and biogeography; Atlantic Ocean, Micropaleontology 24 (1978) 337–370, 10.2307/1485368.
[29] J.W. Hedgpeth, Treatise on Marine Ecology and Paleoecology, The Geological Society of America, Washington, D. C., 1957, 10.1130/MEM67vol. 1.
[30] J.C.J. Ingle, Cenozoic Paleobathymetri and Depositional History of Selected Sequences within the Southern California Continental Borderland, Cushman Fo, Cushman Foundation Special Publication, Kansas, 1980.
[31] J.W. Murray, Distribution and Ecology of Living Benthic Foraminiferids, Crane Russak & Co., New York, 1973, pp. 1011–1012, 10.4319/lo.1973.18.6.1011a.
[32] P. Armas, C. Moreno, M. Lidia, F. González, Journal of south American earth sciences sedimentary palaeoenvironment , petrography , provenance and diagenetic inference of the anacleto Formation in the neuquén basin , late cretaceous , Argentina, J. South Am. Earth Sci. 53 (2014) 59–76, https://doi.org/10.1016/j.jsames.2014.03.004.
[33] A. Maravelis, A. Zelilidis, Petrography and geochemistry of the late Eocene – early Oligocene submarine fans and shelf deposits on Lemnos Island , NE Greece, Implications for provenance and tectonic setting 45 (2010) 412–433, https://doi.org/10.1002/gj.
[34] C.K. Wentworth, A scale of grade and class terms for clastic sediments, J. Geol. 30 (1922) 377–392.
[35] T.C. Blair, J.G. McPherson, Grain-size and textural classification of coarse sedimentary particles, J. Sediment. Res. 69 (1999) 6–19, 10.2110/jsr.69.6.
[36] R.R. Compton, Manual of Field Geology, Jonh Wiley and Sons, Inc, New York, London, 1962.
[37] M.C. Powers, A new roundness scale for sedimentary particles, J. Sediment. Petrol. 23 (1953) 117–119, 10.1306/D4269567-2B26-11D7-8648000102C1865D.
[38] A.G. Maravelis, R. Offler, G. Pantopoulos, W.J. Collins, Provenance and tectonic setting of the Early Permian sedimentary succession in the southern edge of the Sydney Basin, eastern Australia 56 (2021) 2258–2276, https://doi.org/10.1002/gj.4051.

[39] F.J. Pettijohn, P.E. Potter, R. Siever, Sand and Sandstone, Springer-Verlag, New York, Heidelberg, Berlin, 1973, https://doi.org/10.1007/978-1-4615-9974-6.
[40] E. Garzanti, Petrographic classification of sand and sandstone, Earth Sci. Rev. 192 (2019) 545–563, https://doi.org/10.1016/j.earscirev.2018.12.014.
[41] A. Kovani, C. Botziolis, A.G. Maravelis, G. Pantopoulos, G. Iliopoulos, A. Zelilidis, Provenance and statistical analysis of the Lower Oligocene gravelly deposits in central Pindos foreland basin, western Greece : Implications for orogenic build-up and unroofing 58 (1) (2023) 497–521, https://doi.org/10.1002/gj.4608.
[42] W.R. Dickinson, Interpreting Provenance Relations from Detrital Modes of Sandstones, Zuffa, G.G. Proven, Arenites. NATO ASI Ser., 1985, pp. 333–361, 10.1007/978-94-017-2809-6_15.
[43] W.R. Dickinson, L.S. ue Beard, G.R. Brakenridge, J.L. Erjavec, C. Ferguson, K.F. Inman, R.E.X.A. Knepp, F.A. Lindberg, P.T. Ryberg, Provenance of North American Phanerozoic sandstones in relation to tectonic setting Provenance of North American Phanerozoic sandstones in relation to tectonic setting, Geol. Soc. Am. Bull. 94 (1983) 222–235, 10.1130/0016-7606(1983)94<222:PONAPS>2.0.CO;2.
[44] S. Fans, C. Systems, L. Science, S.G. Ecology, L. Editor, J.A. Covault, N.E. Citation, S. Fans, C. Systems, Submarine fans and canyon-channel systems : a review of processes , products , and models A review of processes , products , and models, Nat. Educ. Knowl. (2016) 1–13.
[45] A. Maravelis, P. Konstantopoulos, G. Pantopoulos, A. Zelilidis, North aegean sedimentary basin evolution during the late eocene to early Oligocene based on sedimentological studies on lemnos island (NE Greece), Geol. Carpathica 58 (2007) 455–464.
[46] M. Madon, Submarine mass-transport deposits in the semantan formation (Middle-Upper triassic), central peninsular Malaysia, Bull. Geol. Soc. Malays. (2010) 15–26, https://doi.org/10.7186/bgsm56201003.
[47] G. Shanmugam, Deep-water processes and facies models: implications for sandstone petroleum reservoirs, in: Handbook of Petroleum Exploration and Production, first ed., Elsevier, 2006.
[48] H.H. Ismail, M. Madon, Z.A. Abu Bakar, Sedimentology of the semantan formation (middle - upper triassic) along the karak-kuantan highway, central pahang, Bull. Geol. Soc. Malays. 53 (2007) 27–34, https://doi.org/10.7186/bgsm53200706.
[49] R.G. Walker, Generalized facies models for resedimented conglomerates of turbidite association, Bull. Geol. Soc. Am. 86 (1975) 737–748, https://doi.org/10.1130/0016-7606(1975)86<737:GFMFRC>2.0.CO, 2.
[50] M.N.I.A. Rahman, H. Jeofry, M. Abdulla, I.A. Rahim, S.H. Tahir, Facies analysis of the late eocene deep-marine middle-to outer-fan sequence of the crocker formation in Tenom district, Sabah, Malaysia, Bull. Geol. Soc. Malays. 72 (2021) 47–62, https://doi.org/10.7186/bgsm72202105.
[51] D. Stow, Z. Smillie, Distinguishing between deep-water sediment facies, Geosciences 10 (2020) 1–43, 10.3390/geosciences10020068.
[52] (n.d.). www.mikrotax.org. (Accessed 12 June 2023). www.mikrotax.org.
[53] A. Holbourn, A.S. Henderson, N. Macleod, Atlas of Benthic Foraminifera, Edition First, Wiley-Blackwell, Oxford, 2013.
[54] J.W. Murray, Ecology and Applications of Benthic Foraminifera, Cambridge University Press, Cambridge, UK, 2006, 10.1017/CBO9780511535529.
[55] M.E. Tucker, An Introduction to the Origin of Sedimentary Rocks, 1991.
[56] A. Basu, S.W. Young, L.J. Suttner, W.C. James, G.H. Mack, Re-evaluation of the use of undulatory extinction and polycrystallinity in detrital quartz for provenance interpretation, J. Sediment. Petrol. 45 (1975) 873–882, 10.1306/212F6E6F-2B24-11D7-8648000102C1865D.
[57] S.W. Young, Petrographic textures of detrital polycrystalline quartz as an aid to interpreting crystalline source rocks, SEPM J. Sediment. Res. 46 (1976) 595–603, https://doi.org/10.1306/212f6ffa-2b24-11d7-8648000102c1865d.
[58] W.L. Brown, I. Parsons, Feldspars in igneous rocks, in: Feldspars Their React, Springer, Dordrecht Heidelberg New York London, 1994, pp. 449–499, https://doi.org/10.1007/978-94-011-1106-5_12.
[59] S. Morad, Feldspars in sedimentary rocks, in: G.V. Middleton, M.J. Church, M. Coniglio, L.A. Hardie, F.J. Longstaffe (Eds.), Encyclopedia of Sediments and Sedimentary Rocks. Encyclopedia of Earth Sciences Series, Springer Link, Kluwer Academic Publishers, Dordrecht, The Netherlands, 2003, 10.1007/978-1-4020-3609-5_84.
[60] E.D. Pittman, Use of Zoned Plagioclase as an Indicator of Provenance 33 (1963) 380–386, 10.1306/74D70E61-2B21-11D7-8648000102C1865D.
[61] I.S. Sanders, J.H. Morris, Evidence for caledonian subduction from greywacke detritus in the longford-down inlier author (s): I . S . Sanders and J . H . Morris, J. Earth Sci. 1 (1978) 53–62.
[62] W.R. Dickinson, C.A. Suczek, Plate tectonics and sandstone composltlons, Am. Assoc. Pet. Geol. Bull. 63 (1979) 2164–2182.
[63] A.J. Barber, M.J. Crow, Chapter 4 pre-tertiary stratigraphy, Geol. Soc. London, Mem 31 (2005) 24–53, https://doi.org/10.1144/GSL.MEM.2005.031.01.04.
[64] Google earth. https://Earth.Google.Com, 2023.
[65] R.P. Koesoemadinata, An Introduction into the Geology of Indonesia, First, Ikatan Alumni Geologi Institut Teknologi Bandung, Bandung, 2020.
[66] Z.A. Kamili, J. Kingston, Z. Achmad, A. Wahab, S. Sosromihardjd, C.U. Crausaz, Contribution to the pre–baong stratigraphy of North Sumatra, 5th Annu. Conv. Proc. 2 (1976) 91–108.
[67] M.C. Daly, M.A. Cooper, I. Wilson, D.G. Smith, B.G.D. Hooper, Cenozoic plate tectonics and basin evolution in Indonesia, Mar. Petrol. Geol. 8 (1991) 2–21, https://doi.org/10.1016/0264-8172(91)90041-X.
[68] A.C. Morton, B. Humphreys, D.A. Dharmayanti, Sundoro, palaeogeographic implications of the heavy mineral distribution in Miocene sandstones of the North Sumatra basin, J. Southeast Asian Earth Sci. 10 (1994) 177–190, https://doi.org/10.1016/0743-9547(94)90018-3.
[69] N.R. Cameron, M.C.G. Clarke, D.T. Aldiss, J.A. Aspden, A. Djunuddin, The geological evolution of Northern Sumatra, in: Proc. Indones. Pet, . Assoc., 1980, https://doi.org/10.29118/ipa.619.149.187.
[70] G.L. De Coster, The geology of the central and South Sumatra basins, in: Proc. Indones. Pet. Assoc., 1974, https://doi.org/10.29118/ipa.670.77.110.
[71] S. Mertosono, G.A.S. Nayoan, The tertiary basinal area of central Sumatra, in: Proc. Indones. Pet. Assoc., 1974, pp. 63–76.
[72] J.N. Spruyt, Subdivisions and Nomenclature of the Tertiary, Sediments of the Djambi-Palembang Area, Pertamina Internal Report., 1956.